

Vortices in rotating Bose gas interacting via finite range
Gaussian potential in a quasi-two-dimensional harmonic trap

Md Hamid^{1,*} and M. A. H. Ahsan¹

¹*Department of Physics, Jamia Millia Islamia (A
Central University), New Delhi 110025, India*

(Dated: April 4, 2025)

Abstract

A system of harmonically trapped $N=16$ spin-0 bosons confined in quasi-2D symmetrical $x - y$ plane interacting via a finite range repulsive Gaussian potential is studied under an externally impressed rotation to an over all angular velocity Ω about the z -axis. The exact diagonalization (ED) of $n \times n$ many-body Hamiltonian matrix in a given subspace of quantized total angular momentum $0 \leq L_z \leq 4N$ is performed using Davidson algorithm. For $N = 16$ and $L_z = 32$, the dimensionality of the Hilbert space turns out to be $n = 384559$. With increase in the interaction range in the Gaussian potential, the active Fock space size gets reduced and hence computation becomes more feasible compared to the zero-range δ -function potential. Following this idea, we considered the interaction-range parameter $\sigma = 0.30, 0.50$ and 0.75 to study the finite-range effects on the many-body ground state. The trap velocity Ω being the Lagrange multiplier associated with the angular momentum L_z for the rotating systems, the $L_z - \Omega$ phase diagram (or stability line) is drawn which determines the critical angular velocities, $\Omega_{c_i}, i = 0, 1, 2, \dots$, at which, for a given angular momentum L_z , the system goes through a quantum phase transition. Further with increase in interaction range σ , the quantum mechanical coherence extends over more and more particles in the system resulting in an enhanced stability of the i^{th} vortical state with angular momentum $L_z(\Omega_{c_i})$ leading to a delayed onset of the the next vortical state $L_z(\Omega_{c_{i+1}})$ at a higher value of the next critical angular velocity $\Omega_{c_{i+1}}$. There is an increase in the critical angular velocity ($\Omega_{c_i}, i = 1, 2, 3 \dots$) and in the largest condensate fraction λ_1 , calculated using single particle reduced density matrix (SPRDM) eigen-values with increase in the interaction range σ . We calculated the von-Neumann quantum entropy (S_1), degree of condensation (C_d) and the conditional probability density (CPDs). There is no significant change in von-Neumann entropy S_1 and the degree of condensation C_d in slow-rotating gas in the region $0 \leq L_z \leq (L_z = N)$. However, for higher angular momentum, $L_z \geq 2N$, with increase in interaction range σ , small variations in S_1 and C_d are observed. We plot the isosurface CPDs

plots for conditional probability and hence study the nucleation of vortex states, which is one of the signature of rotating bose gas, we report that with the increase in interaction range σ , the probability density starts accumulation at the edge of vortices. Accumulation of density at the surfaces of sphere in the case of Bose-condensate in the bubble trap has been discussed here [1]. We also observed that the vortices entry started for the higher σ followed by the lower. We plotted the CPDs to study $p = 1, 2, 3, 4, 5$ fold symmetrical vortex lattices. Concluding we suggest the modification of single particles basis state with the increase in σ at $L_z = 32$, $\sum_{i=1,3}(n_i, m_i)(\sigma = 0.30) [(2, 2), (0, 0), (4, 4)]$, $\sum_{i=1,3}(n_i, m_i)(\sigma = 0.50) [(2, 2), (0, 0), (4, 4)]$ and $\sum_{i=1,3}(n_i, m_i)(\sigma = 0.75) [(2, 2), (3, 3), (1, 1)]$.

* hamidjmi2008@gmail.com

I. INTRODUCTION

The achievement of Bose-Einstein condensates (BECs) in harmonically trapped atomic vapours has stimulated explosively growing interest in the system of interacting bosons [2–11] and for the parabolic trap is studied for contact potential. Theoretical studies in quasi-two dimensions are mainly focused on the rotating properties and vortex structure in BEC. The presence of vortex states is a signature of macroscopic phase coherence state moreover vortices are the signature of superfluidity of the Bose Einstein condensate state. Quantized vortices have been studied for the superfluid ^4He as the topological defects behaviour of superfluid [12]. For weakly interacting Bose gas, vortex states are not stable and become unstable with the halt of externally impressed rotation, such state can't be the superfluid, on the other hand when interaction and trap effects become comparable, we find interesting symmetry breaking (SB) instability which modifies vortex core and induces precession about the axis of trap [13, 14]. Experiments with Alkali atoms such as ^{23}Na , ^{39}K , ^{87}Rb and ^7Li (attractive interaction [15]) confined in magnetic traps and cooled down to 100 nK have been achieved in laboratories have sustained the interest in the BECs [16–18]. By using the focused laser beam, Madison et al. has stirred the ^{87}Rb atom to observe the vortex at stirred angular velocity exceeding the critical angular velocity Ω_c , till the four vortices presented simultaneously [19]. In the usual ultra-cold atomic gases experiments, the atom-atom interaction is well modelled by the zero-contact δ potential i.e. $\sigma \rightarrow 0$ [20]. For 1D study the contact zero range δ potential is a suitable choice for contact interactions but for higher dimensions the achieving the convergence of single particle basis states becomes a painful task, finite range Gaussian potential is appropriate in terms of convergence. The sign of finite range Gaussian potential is taken to be positive to make the interaction repulsive [21–23]. For numerical studies, in finite range Gaussian potential we have some advantages in tuning

the inter-particle interaction range σ , to study the finite range effects. The finite range potential, can be expanded within the finite numbers of single particles basis state in contrast to the zero-range δ function, which significantly facilitate the convergence of numerical results, are among the few advantages of finite range Gaussian interaction ($\sigma \rightarrow \infty$) over contact potential ($\sigma \rightarrow 0$). In the present study, we have tuned the interaction range parameter of the finite range Gaussian function in the range from 0.3 to 0.75 within the slow to fast rotating angular momentum in the range $0 \leq L_z \leq 4N$ along the rotation axis- z . For some results we studied $0 \geq \sigma \leq 0.80$ for $L_z = 32$. Our focussed is in the study of the finite range interaction. Most of the theoretical work in the literature have focused on the “lowest-Landau-level” (LLL) approximation, in which single particle orbital states with the radial quantum $n_r = 0$, while single particle angular momentum quantum number m takes positive values (with respect to trap angular velocity Ω along the rotation axis- z). This reduces the dimensionality of the Hilbert space significantly [24–27]. In moderately to strongly interacting regime and slowly rotating system, beyond LLL approximation with $n_r = 0, 1 \dots$ while m is allowed to take both positive and negative values $\pm m$, is considered a better variational approximation over LLL approximation [30]. In fast rotating regime, both LLL and beyond LLL approximations give comparable ground state energy E_0^{lab} and critical angular velocity Ω_c , as is in Tab. VIII. For two-particles interaction range other than $\sigma \rightarrow 0$, the Dirac δ -function is not suitable choice for two-body interaction in exact theories. The exact diagonalization of the Hamiltonian matrix for the finite N-body system yields an exact solution within a finite number of single particle basis. For the numerical feasibility it is necessary to select the single particles basis out of many particle basis to formulate the variational wave-basis. The usual contact δ -potential $g_2 \delta_{\mathbf{r},\mathbf{r}'} = g_2 \sum_{\mathbf{n}} u_{\mathbf{n}}^*(\mathbf{r}) u_{\mathbf{n}}(\mathbf{r}')$, where sum runs over all infinite single particle basis states, therefore is not suitable for the numerically carry out exact diagonalization. Therefore the choice for the finite range smooth Gaussian

potential in Eq. (2) over usual zero-contact range δ -potential in Eq. (3) is preferable which can be expanded within the finite number of single particle basis states. [28, 29]. In order to construct the many-particle basis states, we go beyond the LLL so as to select the single particle basis state that includes the radial quantum number $n_r = 0, 1$ and the single particle angular momentum quantum number m of either sign [30].

We explore the physics of various stable and unstable states in subspace of quantized total angular momentum L_z and their transition to different vortex patterns. For fast rotating case, in the orbital angular momentum range $2N > L_z \leq 4N$, higher p-fold symmetry started to emerge, $p = 3, 4, 5, \dots$. we have triangular lattice for $L_z = 35$, as shown in Fig. 14(f) and $L_z = 36$, in Fig. 14(g), 15(g) and 16(h). As angular momentum L_z grows, the vortex lattices arranged themselves in the patterns of Abrikosov lattices [31, 32]. In the interaction regime, we can not ignore in contribution of kinetic energy even for larger N , since it determines the structure of vortex core. In particular the balance between the kinetic and the interaction energy fixes a typical distance over which the condensate wave function can heal [33].

This paper is organised as follows: In Sec. II, we derive a general Hamiltonian equation for N trapped spin-0 particles interacting via a normalized repulsive Gaussian-shaped two-body interacting potential in quasi-2D harmonic trap exposed to an over-all rotation about an axis of the symmetric plane. Discussed the need to go beyond LLL and set-up many-body wavefunction out of single particle basis state to carry-out the diagonalization of Hamiltonian. In Sec. III, we present our findings followed by the brief introduction about the quantity of interests like the critical angular velocity Ω_{c_i} , single particle reduced density matrix (SPRDM) using variational wavefunction and follows the von-Neumann entropy S_1 , degree of condensation c_d and lastly the conditional probability density (CPD) to study the spatical co-rrrelation of condensed bose gas. In Sec. V, we present the conclusion.

II. THE HAMILTONIAN

We consider a system of $N = 16$ spin-0 bosons, each of mass M in an external harmonic trap, which are interacting via a normalized Gaussian potential in a $x - y$ symmetric two-dimensional plane with an externally impressed rotation $\mathbf{\Omega} = \Omega \hat{z}$ about z -axis, has been studied in the recent years [28, 34–37] are the bench mark for our study. The Hamiltonian of this system in co-rotating frame can be written as,

$$\widehat{\mathbf{H}}^{rot} = \widehat{\mathbf{H}}^{lab} - \widehat{\mathbf{\Omega}} \cdot \widehat{\mathbf{L}}^{lab}$$

here, Ω is the angular velocity and L is the angular momentum along the rotation z -axis.

$$\widehat{\mathbf{H}}^{lab} = \sum_{i=1}^N \left[\frac{\widehat{\mathbf{p}}_i^2}{2M} + \frac{1}{2} M \omega_{\perp}^2 r_{\perp i}^2 \right] + \frac{1}{2} \sum_{i \neq j}^N U(\mathbf{r}_i, \mathbf{r}'_j) \quad (1)$$

the first two terms in Hamilton Eq. (1), corresponds to the kinetic and trap potential energy respectively and the third term is inter-atomic interaction potential. terms used in the above equation has been discussed in the coming sections.

A. INTERACTION POTENTIAL

The pairwise interaction $U(\mathbf{r}, \mathbf{r}')$ is assumed to be Gaussian of the form,

$$U(\mathbf{r}, \mathbf{r}') = \frac{\widetilde{g}_2}{2\pi\sigma^2} \exp \left[-\frac{(r - r')^2}{2\sigma^2} \right] \quad (2)$$

where, $\widetilde{g}_2 = \frac{4\pi\hbar^2 a_s}{M}$ having units of energy \times volume and in dimensionless units it becomes $g_2 = \frac{4\pi a_s}{a_{\perp}}$ is interaction strength.

where, σ (scaled as a_{\perp}) is the two particles interaction range and dimensionless interaction strength $g_2 = \frac{4\pi a_s}{a_{\perp}}$, in terms of s-wave scattering length $a_s = 1000a_0$, where,

$a_0 = 0.05292$ nm, is Bohr radius. The exact diagonalization study of many-body Hamiltonian matrix is carried out in the beyond Landau Level approximation to obtain the low-lying energy spectrum of ultracold Bose gas in a harmonic trap. Our scheme includes both Lowest Landau Level and beyond Lowest Landau Level approximation with single particle angular momentum m with either sign to construct the many body basis states. where, σ being the range of two-body interaction and g_2 measures the interaction strength. In the limit $\sigma \rightarrow 0$, the above Gaussian potential reduces to the usual zero range-contact δ potential of the form

$$U(\mathbf{r}, \mathbf{r}') = g_2 \delta_{\mathbf{r}, \mathbf{r}'} \quad (3)$$

have been used widely in literatures.

B. TRAPPING POTENTIAL

Harmonic trapping along the symmetric $x - y$ plane

$$V(\mathbf{r}) = \frac{1}{2} M (\omega_{\perp}^2 r_{\perp}^2 + \omega_z^2 z^2) \quad (4)$$

where, $r_{\perp} = \sqrt{x^2 + y^2}$, normal radius from the axis of rotation and ω_{\perp} , ω_z are the radial and axial trap frequency respectively of harmonic confinement. According to these trapping frequencies, here we are writing the corresponding harmonic oscillators lengths $a_{\perp} = \sqrt{\frac{\hbar}{M\omega_{\perp}}}$ and $a_z = \sqrt{\frac{\hbar}{M\omega_z}}$, radial and axial trapping lengths respectively. Further rewriting the above Eq. (4) as,

$$V(\mathbf{r}) = \frac{1}{2} M \omega_{\perp}^2 (r_{\perp}^2 + \lambda_z^2 z^2) \quad (5)$$

where, $\lambda_z^2 = \frac{\omega_z^2}{\omega_{\perp}^2}$ is the anisotropic parameter, corresponds to different trap geometries such that

- $\lambda_z \ll 1$, yields an elongated cigar-shaped condensate (prolate).

- $\lambda_z \gg 1$, yields a flattened disk shaped/ pancake condensate (oblate).
- $\lambda_z = 1$, yields a spherical shape condensate.

C. THE SINGLE PARTICLE ENERGY SPECTRUM

The N-body variational wavefunction $\Psi(\mathbf{r}_1, \mathbf{r}_2, \dots, \mathbf{r}_N)$ is constructed as the linear sum of single particle basis-functions $u_{n,m,n_z}(\mathbf{r})$, chosen to be the eigenfunctions of the non-interacting (single-particle) Hamiltonian.

$$\begin{aligned}
H_{sp} = & \frac{1}{2} \left(\frac{-\hbar^2}{m} \nabla_{\perp}^2 + m\omega^2 r_{\perp}^2 \right) - \Omega l_z \\
& + \frac{1}{2} \left(\frac{-\hbar^2}{m} \nabla_z^2 + \lambda_z^2 z^2 \right)
\end{aligned} \tag{6}$$

the above Eq. (6) is identified as the harmonic oscillator Hamiltonian in a rotating frame with l_z being single particle angular momentum along the rotation z-axis. The well know harmonic oscillator eigensolution is of the form $H_{sp} u_{n_z, n_r, m}(r_{\perp} \alpha_{\perp}, \phi) = \epsilon_{n_z, n_r, m} u_{n_z, n_r, m}(r_{\perp} \alpha_{\perp}, \phi)$ has the following form;

$$\begin{aligned}
\epsilon_{n_z, n_r, m} = & (2n_r + |m| + 1)\hbar\omega_{\perp} + (n_z + 1/2)\hbar\omega_z \\
u_{n_z, n_r, m}(r_{\perp} \alpha_{\perp}, \phi) = & \sqrt{\frac{\sqrt{\lambda_z/\pi^3} \alpha_{\perp}^2 n_r!}{2^{n_z} n_z! (n_r + |m|)!}} (r_{\perp} \alpha_{\perp})^{|m|} \\
& \times e^{-\frac{1}{2}(r_{\perp}^2 \alpha_{\perp}^2 + \lambda_z z^2)} e^{im\phi} \\
& \times L_{n_r}^{|m|}(r_{\perp}^2 \alpha_{\perp}^2) H_{n_z}(\sqrt{\lambda_z} z)
\end{aligned} \tag{7}$$

where, n_r is radial quantum number, single particle angular momentum quantum number $m = 0, \pm 1, \pm 2..$ and axial-quantum number n_z . The $L_{n_r}^{|m|}(r_\perp^2 \alpha_\perp^2)$ and $H_{n_z}(\sqrt{\lambda_z} z)$ are associated Laguerre polynomial and is Hermite polynomial respectively. Our system of quasi 2D in which we assumed such that there is no excitation in stiffer z-axis and hence setting the $n_z = 0$ reduced the Eq. (7)

$$\begin{aligned}
u_{n_r, m}(r_\perp \alpha_\perp, \phi) &= \sqrt{\frac{\sqrt{\lambda_z/\pi^3} \alpha_\perp^2 n_r!}{(n_r + |m|)!}} (r_\perp \alpha_\perp)^{|m|} \\
&\times e^{-\frac{1}{2}(r_\perp^2 \alpha_\perp^2 + \lambda_z z^2)} e^{im\phi} \\
&\times L_{n_r}^{|m|}(r_\perp^2 \alpha_\perp^2)
\end{aligned} \tag{8}$$

here, α_z is inverse harmonic oscillator length $= 1/a_\perp$. Quasi 2D harmonic oscillator energy turned out to be,

$$\epsilon_{n_z, n_r, m} = (2n_r + |m| + 1)\hbar\omega_\perp + 1/2\hbar\omega_z \tag{9}$$

to study the LLL approximation we set $n_r = 0$ for which single particle angular momentum takes the values $m \geq 0$ and the choice for $n_r = 0, 1$ corresponds to $m = \pm 1, \pm 2..$ termed as the beyond LLL approximation in the above Eq. (8). The diagonalization of Hamiltonian has been performed in the subspace of L_z . For bosons, the N-body variational wave function can be expanded in the form of symmetrize product of single particles basis states i.e. $\Psi(\mathbf{r}_1, \mathbf{r}_2, ..\mathbf{r}_N) = \sum_\nu C_\nu \Phi_\nu(\mathbf{r}_1, \mathbf{r}_2, ..\mathbf{r}_N)$,

$$\Phi_\nu = \frac{\sum_P P}{\sqrt{N!}} \prod_{\mathbf{k}=0} \left(\frac{\sum_{j=0}^{\mathbf{k}} \nu_j}{\prod_{i=1+\sum_{j=0}^{\mathbf{k}-1} \nu_j} \frac{u_{\mathbf{k}}(\mathbf{r}_i)}{\sqrt{\nu_{\mathbf{k}}!}}} \right) \tag{10}$$

where, C_ν are variational coefficients and P is the permutation of N particle coordinates where as the sum denotes the symmetrization against the particles exchange

referred as Fock terms. The many-body wavefunction $\Phi_\nu(\mathbf{r}_1, \mathbf{r}_2, \dots, \mathbf{r}_N)$, is labelled by the many-body index $\nu \equiv (\nu_0, \nu_1, \dots, \nu_k)$ are the set of single particles quantum numbers $\mathbf{j} \equiv (n_z, n, m)$ and their respective occupancies ν_j . Satisfying the given constraints $\sum_{j=0}^k \nu_j = N$ and $\sum_{j=0}^k \nu_j m_j = L_z$. The single particle angular momentum quantum number m_j , total number of particles N and the total angular momentum quantum number L_z . Calculation of the interaction co-efficient using direct technique is not much favorable over the second quantization, which have been developed for the calculation of matrix elements of the operators between the wavefunction of the form Eq. (10). It is point where we should switch to the second quantization formalism where the occupation numbers becomes the variable of state. Rewriting the Eq. (10), in the second quantization form in the occupation numbers ν_j notation.

$$|\Phi_\nu\rangle \equiv \prod_{\mathbf{j}=0}^{\mathbf{k}} \frac{1}{\sqrt{\nu_j!}} (\hat{b}_{\mathbf{j}}^\dagger)^{\nu_j} |\text{vac}\rangle \equiv |\nu_0 \nu_1 \dots \nu_j \dots \nu_k\rangle \quad (11)$$

Satisfying the given constraints $\sum_{j=0}^k \nu_j = N$ and $\sum_{j=0}^k \nu_j m_j = L_z$. The single particle angular momentum quantum number m_j , total number of particles N and the total angular momentum quantum number L_z with $j \equiv (n_z, n, m)$. With these constraints the size of active Fock space of orders 10^5 is constructed to carry out the numerical calculation on the small workstation of 3.00 GHz processor. and hence the many-body Hamiltonian Eq. (1), can be written in the following forms

$$H^{lab} = \sum_{\mathbf{i}, \mathbf{j}} H_{\mathbf{i}, \mathbf{j}}^{sp} \hat{b}_{\mathbf{i}}^\dagger \hat{b}_{\mathbf{j}} + \frac{1}{2} \sum_{\mathbf{i}, \mathbf{j}, \mathbf{k}, \mathbf{l}} \langle \mathbf{i}, \mathbf{j} | U_{\mathbf{k}, \mathbf{l}}^{\mathbf{i}, \mathbf{j}} | \mathbf{k}, \mathbf{l} \rangle \hat{b}_{\mathbf{i}}^\dagger \hat{b}_{\mathbf{j}}^\dagger \hat{b}_{\mathbf{l}} \hat{b}_{\mathbf{k}} \quad (12)$$

where $\hat{b}^\dagger(\hat{b})$, creates(destroys) an atom in the single particle states Φ_ν . The first term in the second quantized form of Hamiltonian is one-body matrix-elements in Eq. (12), corresponds to the diagonal terms as can be think of eigen-values $\sum_i \epsilon_i N_i$, and the second one is the interaction Hamiltonian in the form of two-body matrix-elements.

In this article for $N=16$ spin-0 bosons, we have calculated the ground state energy-spectrum for total angular momentum, slow to fast rotation, in the range $0 \leq L_z \leq$

$4N$. The Diagonalization of Hamiltonian matrix is performed for each of subspace angular momentum basis state L_z separately. In the single particle basis state $u_{n,m}$, the single particle angular momentum quantum number is chosen as: $m = l_z - n_b, l_z - n_b + 1, \dots, m = l_z - n_b - 1, l_z + n_b$. Where, l_z is defined in the terms of greatest integer function and $n_b = 3, 4$ as the size of single particle basis state depending on the available numerical resources and interaction strength. If we consider $N = 16$ and $L_z = 32$ to following the scheme, we define a greatest integer function $l_z = [L_z/N] = 2$, is defined as the $[x]$, for a given real x , the integer is either less or equal to itself. The example presented here, we choose $n_r = 0, 1$ and $n_b = 3$ for numerical feasibility, the single particles angular momentum takes the values $m = -1, 0, 1, 2, 3, 4$ and the $u_{n,m}$ single particle basis state set turns out to be the following,

$$\{u_{0,0}, u_{1,1}, u_{2,2}, u_{3,3}, u_{4,4}, u_{5,5}, u_{1,-1}, \\ u_{2,0}, u_{3,+1}, u_{4,2}, u_{5,3}, u_{3,-1}\}.$$

These single particle basis states are selected for the construction of the many-particle basis state Φ_ν , in the variational trial wave function $\Psi = \sum_\nu C_\nu \Phi_\nu$ of the system for each total angular momentum L_z in the similar manner for the entire range $0 \leq L_z \leq 4N$.

III. RESULTS FOR A SYSTEM OF FIXED PARTICLES

The results and discussions are presented here for $N = 16$ spin-0 bosons of ^{87}Rb atom confined to a quasi 2D anisotropic harmonic trap with anisotropic in ratio $\lambda_z = \frac{\omega_z}{\omega_\perp} = \sqrt{8}$ with radial frequency $\omega_\perp = 2\pi \times 220$ Hz. This choice of radial frequency corresponds to the trap length $a_\perp = \sqrt{\hbar/(M\omega_\perp)} = 0.727\mu\text{m}$. The particle-particle dimensionless interaction strength turns out to be $g_2 = 0.9151$ corresponding to the s-wave scattering length $a_s = 1000a_0$, where $a_0 = 0.05292$ nm is the Bohr

radius. The condensate has a extension along the vertical axis of dimension $a_z = \sqrt{\hbar/M\omega_z} = a_\perp \lambda_z^{-1/2}$ and its dynamics along this axis is assumed to frozen. For the many-body system under study, the characteristic energy scale is determined in terms of dimensionless parameters (Na_s/a_\perp) corresponding to experimental situation [4]. With the choice of above system parameters, we are dealing with the dilute bose-gas in the limit $\bar{n}a_s^3 = 6.171 \times 10^{-3} \ll 1$ with $\bar{n} \equiv N/a_\perp^3$ being the density of bose-gas. Moreover, the size of the system $a_\perp = 0.727\mu m$ is larger than the healing length $\xi = \frac{1}{\sqrt{8\pi\bar{n}a_s}} = 0.1343$, the minimum characteristic length at which the wave function tends to its bulk value when subjected to the localized perturbation [38]. The characteristics exhibited by our model may, thus, be expected to be suitable for the bulk superfluid [39]. Here we present our study for a range of orbital angular momentum $0 \leq L_z \leq 4N$ and interaction range $\sigma = 0.3, 0.5$ and 0.75 .

A. CRITICAL ANGULAR VELOCITY

For the considered system of $N=16$ spin-0 bosons interacting via a finite range Gaussian potential, the ground state is obtained by minimizing the free energy function $F(T, V, N) = E(S, V, N) - TS$ given by $\exp(-\beta F) = \text{Tr} [\exp\{-\beta(\hat{\mathbf{H}}^{lab} - \Omega\hbar\hat{\mathbf{L}}_z^{lab})\}]$ which at $T = 0$ becomes $E(S = 0, V, N) = \langle \Psi_0 | (\hat{\mathbf{H}}^{lab} - \Omega\hbar\hat{\mathbf{L}}_z^{lab}) | \Psi_0 \rangle = \langle \hat{\mathbf{H}}^{lab} \rangle - \hbar\Omega\langle \hat{\mathbf{L}}_z \rangle$ where Ψ_0 is the simultaneous eigenstate of the Hamiltonian and total angular momentum obtained variationally with total angular momentum L_z in non-rotating frame. Therefore the many-body Hamiltonian \mathbf{H}^{lab} in Eq. (1) is diagonalized in the given subspace of total angular momentum L_z to obtain the minimized energy $E^{rot}(L_z, \Omega, g_2) = E_0^{lab}(L_z, \Omega, g_2) - \hbar\Omega L_z^{lab}$ in the co-rotating frame. This can be seen as the minimization of energy $\langle \mathbf{H}^{lab} \rangle = \langle E_0^{lab} \rangle$ subjected to the constraint that the system has the angular momentum expectation $\hat{\mathbf{L}}_z^{lab}$ with the identification that the angular velocity Ω is the Lagrange multiplier. In the absence of external rotation,

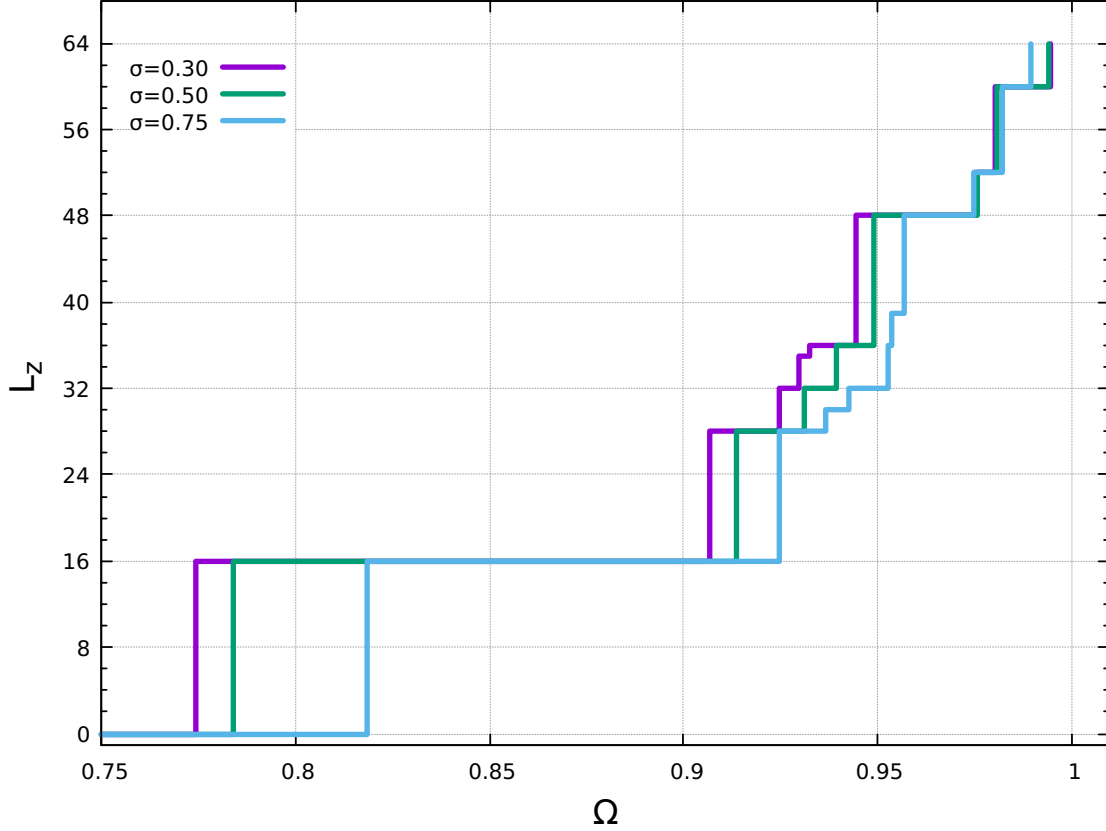


FIG. 1. (Color online) Gives the plot for angular velocity Ω vs the total orbital angular momentum state L_z along rotation axis, for different interaction range σ in the beyond LLL approximation ($n_r = 1$). The horizontal plateaus represents the stability of L_z for the $\Omega_{\mathbf{c}_i}$ and the vertical steps shows the quantum jumps along the different vortical symmetry stable states. In units of ω_{\perp} , \hbar , $\sqrt{\frac{\hbar}{m\omega}}$ respectively.

the angular momentum state $L_z = 0$ corresponds to ground state of the system. When system is subjected to the externally impressed rotation, the non zero angular momentum states $L_z \neq 0$ successively becomes the next ground state. Thus For higher angular velocity $\Omega_{\mathbf{c}_{(i+1)}}$, the corresponding angular momentum state becomes

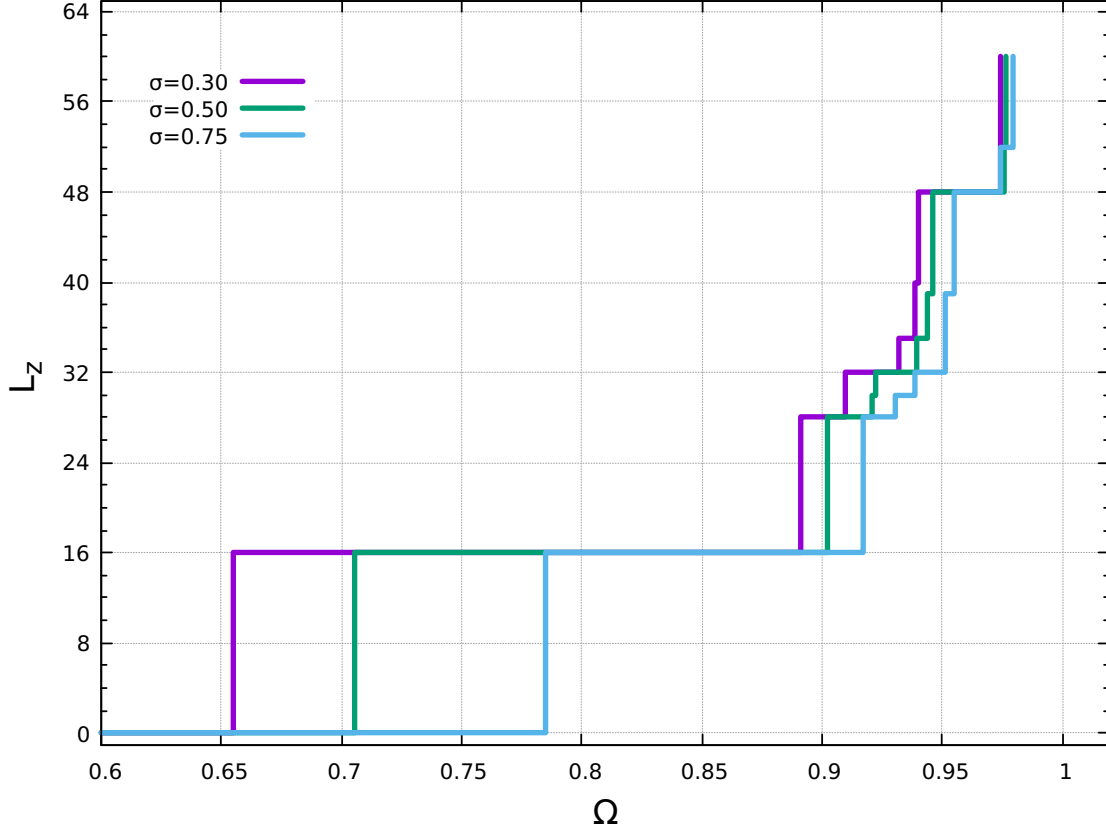


FIG. 2. (Color online) Gives the plot for angular velocity Ω vs the total orbital angular momentum state L_z along rotation axis, for different interaction range σ in the LL approximation ($n_r = 0$). The horizontal plateaus represents the stability of state L_z for the $\Omega_{\mathbf{c}_i}$ and the vertical steps shows the quantum jumps along the different vortical symmetry stable states. In units of ω_\perp , \hbar , $\sqrt{\frac{\hbar}{m\omega}}$ respectively.

the ground state in energy. Following this scheme we can have a set of critical angular velocities $\{\Omega_{\mathbf{c}_i}(L_z, U(r)), i = 1, 2, 3, \dots\}$ at which there is an abrupt quantum jump in the quantized angular momentum L_z of the rotating system given by the

below expression Eq.(13).

$$\Omega_{\mathbf{c}} \left(L_z^i, U(r) \right) = \frac{E_0^{lab} \left(L_z^i, g_2 \right) - E_0^{lab} \left(L_z^{(i-1)}, g_2 \right)}{L_z^i - L_z^{(i-1)}} \quad (13)$$

where, $E_0^{lab} (L_z^i, g_2, \sigma,)$ is interacting ground state energy in laboratory frame under rotation $L_z^i(\Omega)$ of i -th particle angular momentum, interaction range σ and interaction strength g_2 . The stability line in Fig. 1 has a series of discrete jumps at the critical angular velocities $\{\Omega_{\mathbf{c}_i}, i = 1, 2, \dots\}$ and corresponding plateaus at L_z^i with increase in angular momentum in the range $0 \leq L_z \leq 4N$. We observe that the angular momentum state $L_z = 0$ remains the ground state of the system till the angular velocity attains the first critical value $\Omega_{\mathbf{c}_1}$. As the system is subjected to further rotation, higher angular momentum states $L_z > 0$, which minimize the free energy $E^{lab} - \hbar L \Omega$ in the co-rotating frame, become the successive ground states of the system at a series of critical angular velocities $\{\Omega_{\mathbf{c}_i}, i = 1, 2, \dots\}$. We note that for a given value of interaction strength g_2 , the respective critical angular velocities increase for increasing values of the interaction range σ in slowly to moderately rotating regime *e.g.* $\Omega_{\mathbf{c}_1}(\sigma = 0.3) < \Omega_{\mathbf{c}_1}(\sigma = 0.50) < \Omega_{\mathbf{c}_1}(\sigma = 0.75)$ as seen in Fig. 1. This can be understood as follows: with increase in interaction range σ , the quantum mechanical coherence extends over more and more particles in the system resulting in an enhanced stability of the i^{th} vortical state with angular momentum $L_z(\Omega_{\mathbf{c}_i})$ leading to a delayed onset of the next vortical state $L_z(\Omega_{\mathbf{c}_{i+1}})$ at a higher value of the next critical angular velocity $\Omega_{\mathbf{c}_{i+1}}$. We observe jumps in the total angular momentum state of the ground-state at characteristic critical angular velocities $\{\Omega_{\mathbf{c}_i}(L_z), i = 1, 2, \dots\}$. For the non-rotating $L_z = 0$ state, the critical angular velocity for various values of σ are: $\Omega_{\mathbf{c}_1}^{\sigma=0.30} = 0.774$, $\Omega_{\mathbf{c}_1}^{\sigma=0.50} = 0.784$ and $\Omega_{\mathbf{c}_1}^{\sigma=0.75} = 0.818$. The plateaus in

the L_z state are found at $\Omega \rightarrow \Omega_{\mathbf{c}_i}$. These ground state in L_z (plateaus) are being maintained till the entry of next vortical state at $L_z(\Omega_{\mathbf{c}_{i+1}})$. Second quantum jump for the single vortex state at $L_z = 16 = N$ for the various values of σ are: $\Omega_{\mathbf{c}_2}^{\sigma=0.30} = 0.907$, $\Omega_{\mathbf{c}_2}^{\sigma=0.50} = 0.914$ and $\Omega_{\mathbf{c}_2}^{\sigma=0.75} = 0.925$. Thus obtained a series of quantum jumps and corresponding vortical states at the critical angular velocities with decreased in plateaus size and step length for a given interaction range σ and strength g_2 . Similar observations is also reported for few-body system in the LLL approximation for δ potential [41]. This is also noted that $\Omega_{\mathbf{c}_i}(L_z, g_2, \sigma)$ decreases with increase in number of particles and interaction strength g_2 [30]. Complete series of quantum jumps and plateaus for $L_z^i(\Omega_{\mathbf{c}_i})$ state for different interaction range σ is given here for the system under study, can be seen in Fig. 1,

$$L_z^i(\sigma = 0.30) = 0, 16, 28, 32, 35, 36, 48, 52, 60.$$

$$L_z^i(\sigma = 0.50) = 0, 16, 28, 32, 36, 48, 52, 60.$$

$$L_z^i(\sigma = 0.75) = 0, 16, 28, 30, 32, 36, 39, 48, 52, 60.$$

similar trends are reported in these articles [40–42] for δ potential in the Lowest Landau Level(LLL) approximation. We can connect these $\Omega_{\mathbf{c}_i}(L_z, g_2, \sigma) \{i = 1, 2, 3 \dots\}$ to the vortex nucleation, degree of condensation and to the von-Nuemann quantum entropy. Number of vortical states increase with increase in the number of micro-plateaus and it is proportional to the vorticity m as indicated in Tab. III,IV and V. Few more higher order p-fold symmetrical vortices for different σ along with $L_z(\Omega_{\mathbf{c}_i})$ for the system in slow rotating regime $0 \leq L_z \leq 2N$ are discussed here, p = 2 fold-vortical states appear at $L_{28}^{(2)}(\sigma = 0.30) = L_{28}^{(2)}(\sigma = 0.50) = L_{28}^{(2)}(\sigma = 0.75)$. In the moderately rotating angular momentum L_z , p = 3 fold symmetrical vortex appears at $L_{32}^{(3)}(\sigma = 0.30) = L_{32}^{(3)}(\sigma = 0.50) = L_{30}^{(3)}(\sigma = 0.75)$ and the p = 4 fold at $L_{35}^{(4)}(\sigma = 0.30) = L_{36}^{(4)}(\sigma = 0.50) = L_{32}^{(4)}(\sigma = 0.75)$. The first and second p fold vortices appeared at the same $L_z(\Omega_{\mathbf{c}_i})$ irrespective of interaction range σ however higher

vortices has different σ and angular momentum states $L_z(\Omega_{\mathbf{c}_i})$ in the selected region. As we mentioned above that the transition of ground state angular momentum from zero to state $L_z = N$ corresponds to the first on-centered vortex and $L_z > 16$ corresponds to the off-centred multi-vortical states, detailed in section IV C 2. The single particle wave-function constructed with odd m satisfied the Jastrow form defined quantum Hall effect [43]. The each ground state corresponding to $\Omega_{\mathbf{c}_i}(L_z, g_2, \sigma)$ are referred as the stable phase-coherent vortices [44, 45]. In ultra-fast rotating regime, the critical angular velocity $\Omega_{\mathbf{c}_i}(L_z, g_2, \sigma)$ becomes independent if interaction range and have coinciding plateaus with same trap height where the rotation motion dominates over the finite range interaction. These are finite range effects in rotating bose-gas, quantum mechanically stable phase-coherent vortical states changed with the interaction range σ in co-rotating frame. The depletion in the condensate is observed to be increased with the increase in L_z as the scattering of particles increased.

B. SINGLE PARTICLE REDUCED DENSITY MATRIX

The single particle reduced density matrix (SPRDM) is an useful tool to study the BECs of the finite system and more then that it is a criterion for the BECs of interacting gas. Since the experimental realization of BECs in dilute gases, efforts has been made to characterize it microscopically. For non-interacting gases, one of the criteria is that the occupation number for one of the single particle energy level should be macroscopic. For interacting gases, criterion was suggested Penrose[46] and Landau[47] later elaborated by Penrose-Onsager[48, 49] and Yang[50]. For many-body problem, SPRDM provides information about dipole moment, absorption spectra and momentum distribution etcetera. To calculate the SPRDM, $\rho_1(\mathbf{r}, \mathbf{r}')$ we integrate out $N - 1$ co-ordinates of varitionally obtained many-body ground state

wave-function $\Psi_0(\mathbf{r}_1, \mathbf{r}_2, \dots, \mathbf{r}_N)$ through the exact-diagonalization is defined as

$$\begin{aligned}
\rho_1(\mathbf{r}, \mathbf{r}') &\equiv \int \int \dots \int d\mathbf{r}_2 d\mathbf{r}_3 \dots d\mathbf{r}_N \\
&\quad \Psi_0^*(\mathbf{r}, \mathbf{r}_2, \mathbf{r}_3 \dots, \mathbf{r}_N) \Psi_0(\mathbf{r}', \mathbf{r}_2, \mathbf{r}_3 \dots, \mathbf{r}_N) \\
&= \sum_n \sum_m \sum_{n_z} \sum_{n'} \sum_{m'} \sum_{n'_z} \rho_{nmn_z, n'm'n'_z} \\
&\quad u_{n,m,n_z}^*(r) u_{n',m',n'_z}(r')
\end{aligned} \tag{14}$$

where, $\rho_{nmn_z, n'm'n'_z} = c_{nmn_z} c_{n'm'n'_z}^*$

for harmonically trapped finite systems, such as in our case, this Eq. (14), can be expended in the forms of eigenfunctions,

$$\rho_1(\mathbf{r}, \mathbf{r}') = \sum_{\mu=1,2,3\dots} \lambda_\mu \chi_\mu^*(\mathbf{r}) \chi_\mu(\mathbf{r}') \tag{15}$$

where, $\{\lambda_\mu\}$ which are eigenvalues (since the density matrix is Hermitian and positive definite so its eigenvalues are positive and real, normalized to $\sum_\mu \lambda_\mu = 1$) and $\{\chi_\mu(r)\}$ is corresponding eigenvectors of $\rho_1(\mathbf{r}, \mathbf{r}')$. The single particle density profile of the system is given by the diagonal part of SPRDM, $\rho_1(\mathbf{r}, \mathbf{r}) \equiv \rho(\mathbf{r})$. If state is pure condensate, then in this case only one largest eigenvalue ($\lambda = 1$) remains significant i.e. von-Neumann entropy $S_1 \rightarrow 0$, which will be discussed in details in coming sections. In the case of fragmented condensate more then one eigenvalues of SPRDM $\lambda_1 \approx \lambda_2 \approx \lambda_3 \approx \dots$ are significantly comparable, where indices are the labelled as quantum numbers corresponding the fragmented condensate. The fragmentation becomes a possible reality in the present case of finite number interacting dilute alkali vapours in harmonically trapped system of different parameters like interaction strength g_2 , interaction range σ , orbital angular momentum L_z or angular velocity Ω , may favours the a commutation relation $[\widehat{N}, \widehat{\Theta}] = \hbar$, between the particles number \widehat{N}

and phase operator $\hat{\Theta}$. Our observations suggested that for $\sigma = 0.75$, the $\lambda_1 \equiv \lambda_2$ at $L_z(\sigma = 0.75) = 12, 23, 35, 46$, and 58 shown in Fig. 8. The fragmented ground state can also be viewed as the expectation over symmetry broken ground states [51, 52].

For our quasi-2D systems, the z-dimension in SPRDM has been traced out and hence setting $n_z = 0$, Eq. (15) reduces to

$$\rho_1(r_\perp \phi; r'_\perp, \phi) = \sum_{\mu=1,2,3\dots} \lambda_\mu \chi_\mu^*(r_\perp \phi; r'_\perp, \phi) \chi_\mu(r_\perp \phi; r'_\perp, \phi) \quad (16)$$

where, $\mu \equiv \{n, m, n_z\}$.

$$\chi_\mu(r_\perp, \phi) = \sum_n c_{n, m_\mu, 0}^\mu u_{n, m_\mu, 0}(\mathbf{r}, \phi)$$

where $|c_{n, m_\mu, 0}^\mu|^2$ in the weight function. SPRDM eigenvectors can be redefined in terms of phase factor single particle basis function as, becomes,

$$\chi_\mu(r_\perp, \phi) = \sum_n \left(c_{n, m_\mu, 0}^\mu f_{n, m_\mu}(r_\perp) \right) e^{im_\mu \phi}$$

where, $n = 2n_r + |m|$

$$f_{n_r, m_\mu}(r_\perp) = \sqrt{\frac{\alpha_\perp^2 n_r!}{\pi(n_r + m_\mu)!}} (r_\perp \alpha_\perp)^{|m_\mu|} e^{-1/2 r_\perp^2 \alpha_\perp^2} \\ \times L_{n_r}^{|m_\mu|}(r_\perp^2 \alpha_\perp^2)$$

the n_μ takes values in steps of m_μ with difference of two ($n = 0, m_1 = 0$) and ($n = 2, m_2 = 0$) which can be seen from Tables III, IV and V, where vorticity m_μ remains constant for the quantum number n . The constraint on total angular momentum as the empirical sum rule follows,

$$L_z = N \sum_\mu m_\mu \lambda_\mu \quad (17)$$

for a harmonically rotating trap. where, m_μ can takes both sign, $0, \pm 1, \pm 2..$, the angular momentum is conserved in fragmented condensate, for a rotating system in a harmonic trap Eq. (17) and (17) have been verified through our computational schemes.

The eigenvector $\chi_1(\mathbf{r}) = \sum c_n^1 u_n(\mathbf{r})$ which is the macroscopic parameter in the mean-field Gross-Pitavaskii systems. From Fig. 6-8, the largest condensate fraction i.e. λ_1 at L_z for σ is listed below. for details see Fig. 9. The condensate depletes

L_z	$\lambda_1(\sigma = 0.30)$	$\lambda_1(\sigma = 0.50)$	$\lambda_1(\sigma = 0.75)$
0	0.989	0.993	0.997
16	0.875	0.879	0.883
32	0.435	0.481	0.639
48	0.484	0.479	0.468
60	0.493	0.501	0.505

with increase in L_z for a given interaction range σ and increases with the increase in the σ .

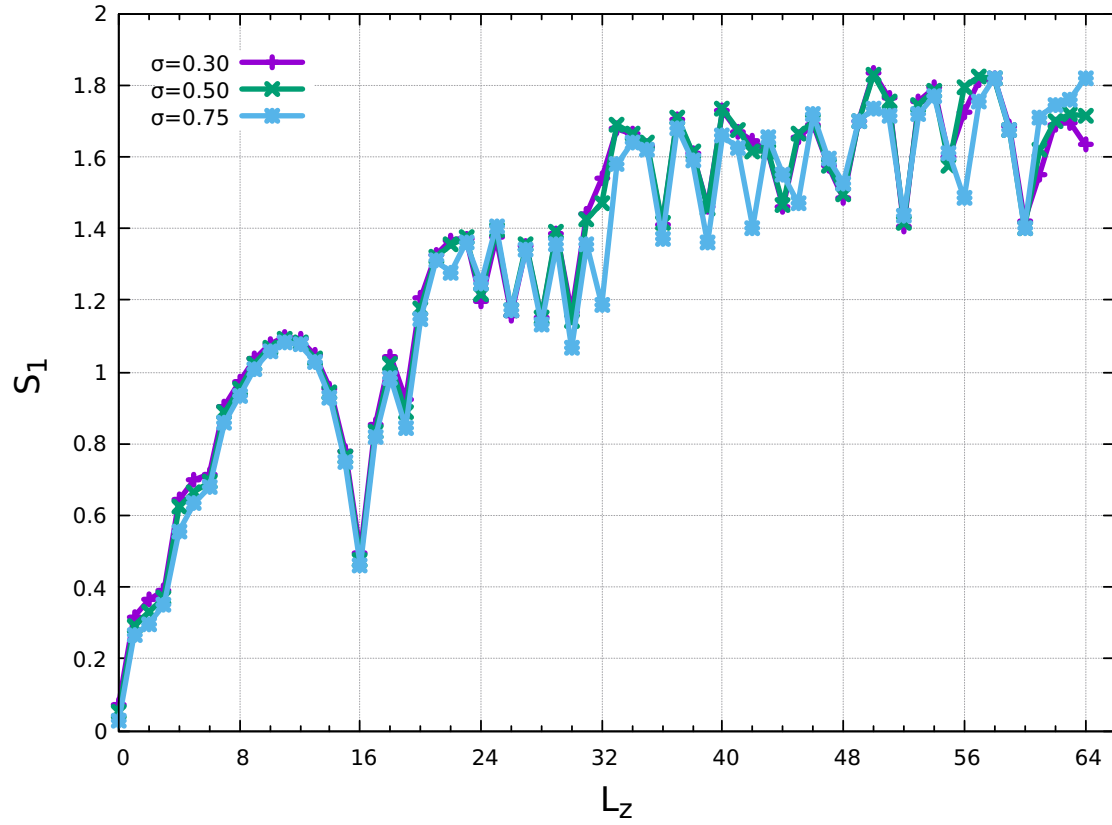


FIG. 3. (Color online) For $N=16$ bosons, the von-Nuemann entropy S_1 vs L_z , total orbital angular momentum in the range of $0 \leq L_z \leq 4N$ for the interaction range $\sigma = 0.30, 0.50$ and 0.75 and interaction strength $g_2 = 0.9151$ of the Gaussian potential Eq. (1).

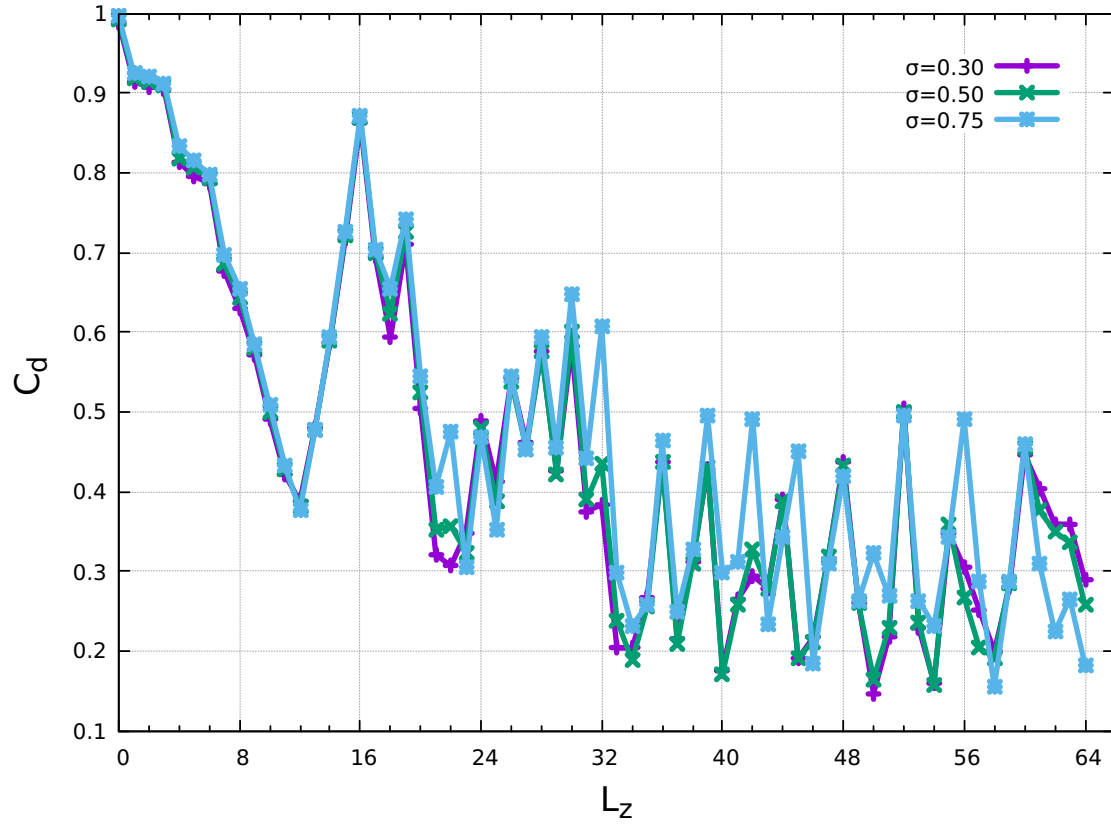


FIG. 4. (Color online) For $N=16$ bosons, the Degree of condensation C_d vs L_z , total orbital angular momentum in the range of $0 \leq L_z \leq 4N$ for the interaction range $\sigma = 0.30, 0.50$ and 0.75 and interaction strength $g_2 = 0.9151$ of the Gaussian potential Eq. (1).

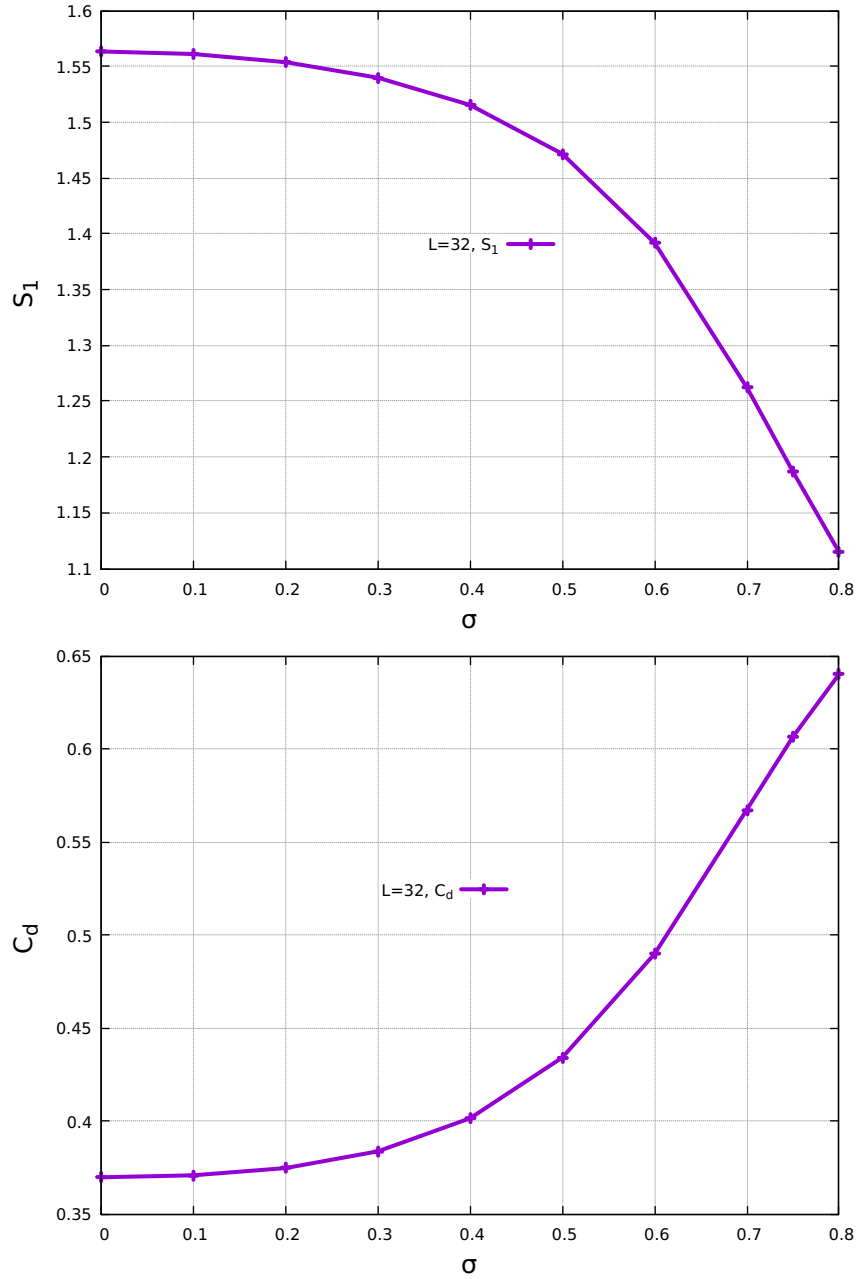


FIG. 5. (Color online) Gives the plot for von-Neumann entropy S_1 and degree of condensation C_d vs interaction range σ for the orbital angular momentum state $L_z = 32$ along rotation axis, and 2-D interaction strength $g_2 = 0.9151$.

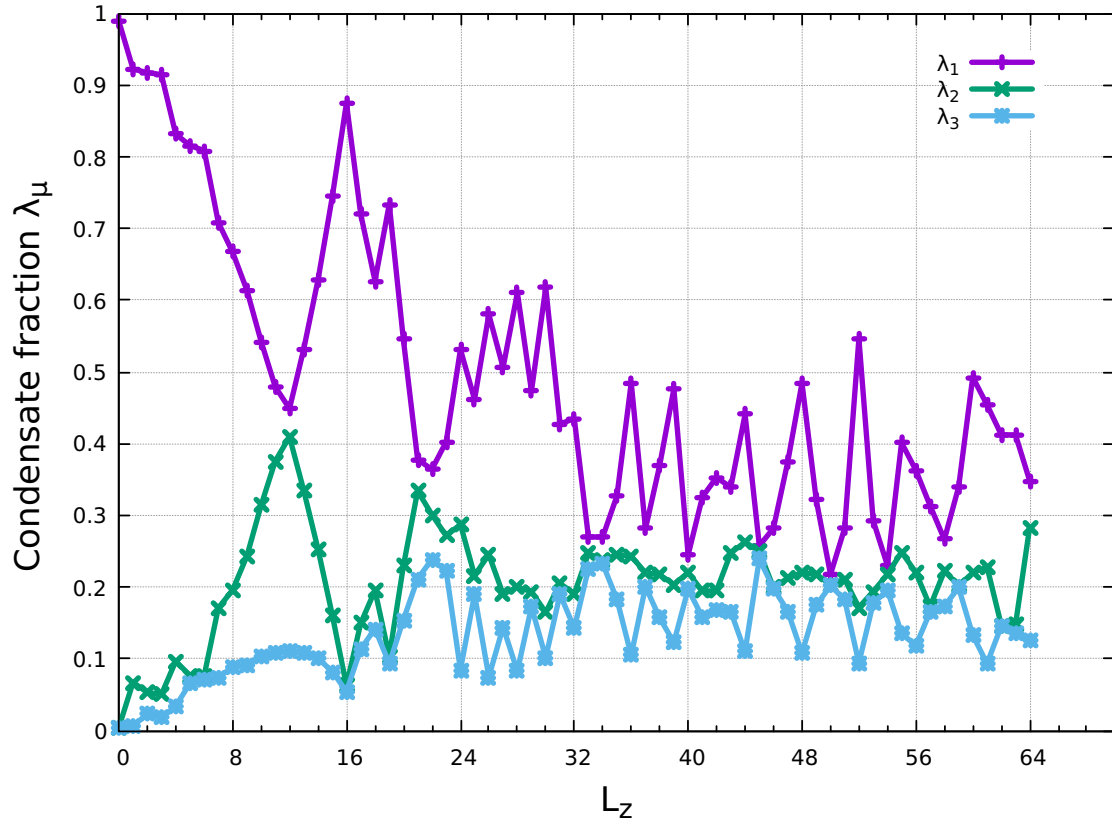


FIG. 6. (Color online) For $N=16$ bosons, plot for condensate fraction λ_μ vs total orbital angular momentum state L_z about the rotation axis, such that $\lambda_1 \geq \lambda_2 \geq \lambda_3$, for interaction range $\sigma = 0.30$, 2-D interaction strength $g_2 = 0.9151$, in the regime $0 \leq L_z \leq 4N$.

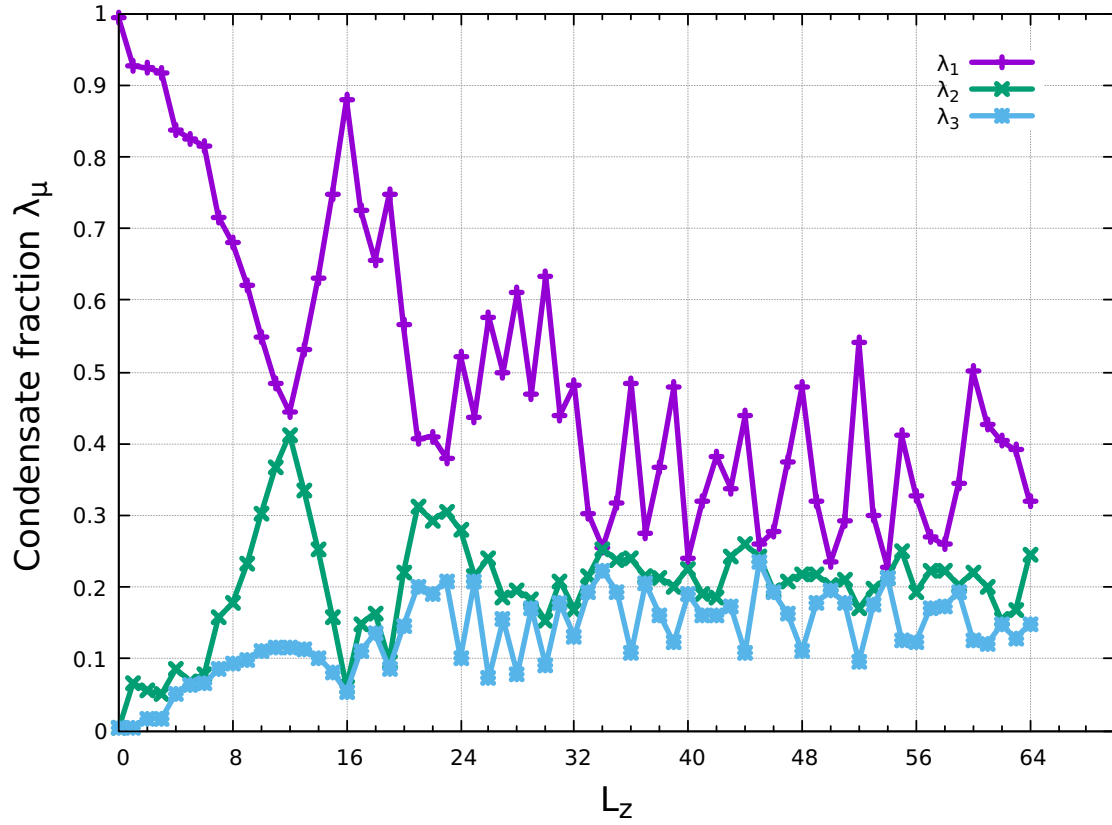


FIG. 7. (Color online) For $N=16$ bosons, plot for condensate fraction λ_μ vs total orbital angular momentum state L_z about rotation axis, such that $\lambda_1 \geq \lambda_2 \geq \lambda_3$, for interaction range $\sigma = 0.50$, 2-D interaction strength $g_2 = 0.9151$, in the regime $0 \leq L_z \leq 4N$.

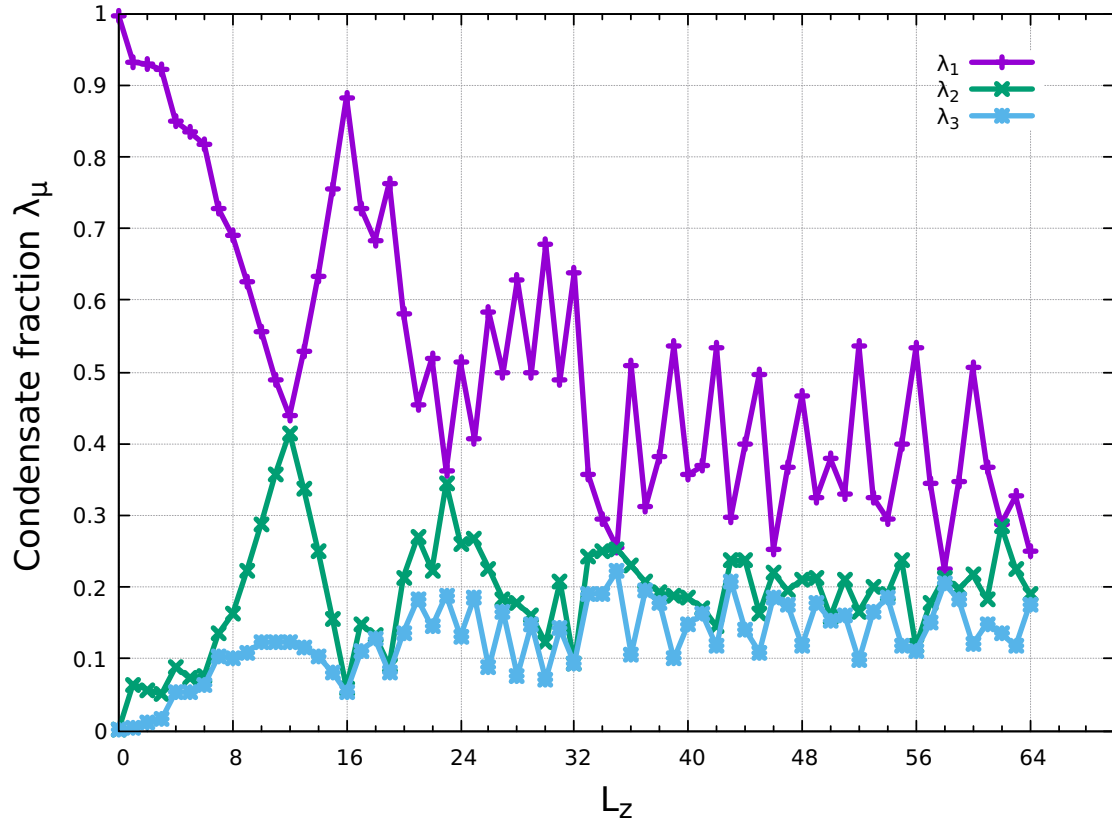


FIG. 8. (Color online) For $N=16$ bosons, plot for condensate fraction λ_μ vs L_z , total orbital angular momentum about rotation axis, such that $\lambda_1 \geq \lambda_2 \geq \lambda_3$, for interaction range $\sigma = 0.75$, 2-D interaction strength $g_2 = 0.9151$, in the regime $0 \leq L_z \leq 4N$.

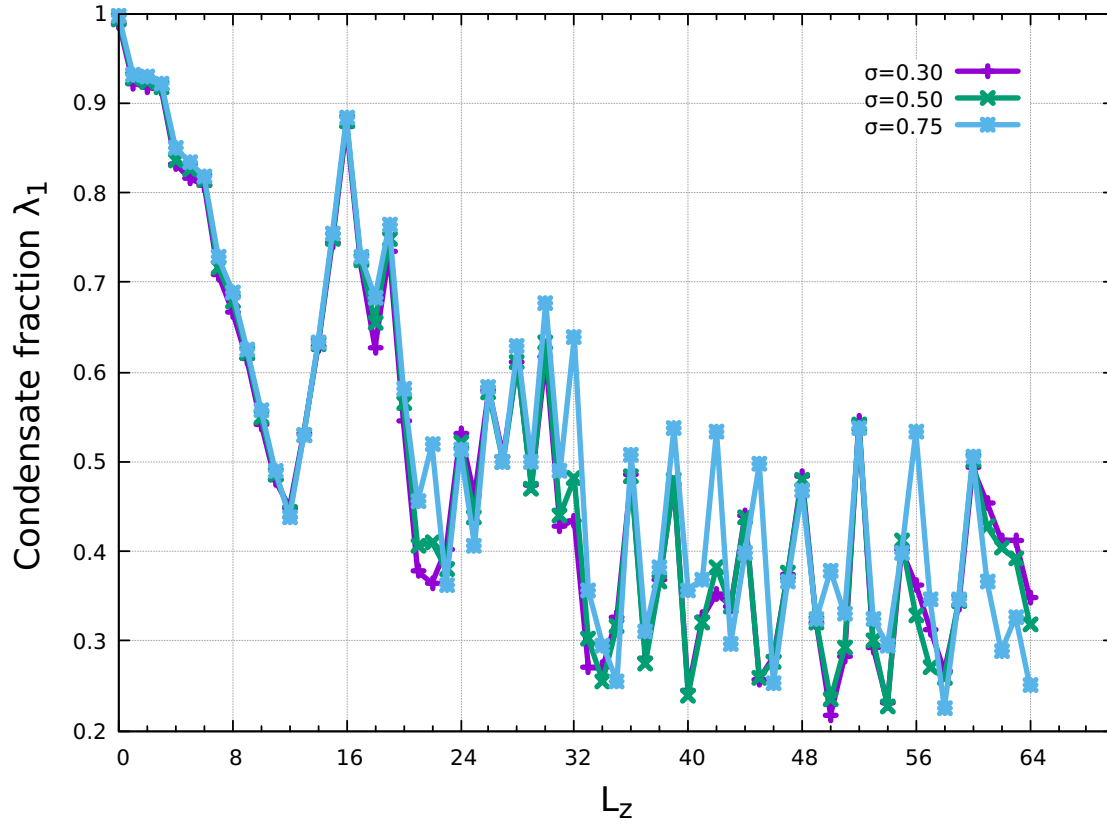


FIG. 9. (Color online) For $N=16$ bosons, plot for condensate fraction λ_1 vs total orbital angular momentum state L_z about the rotation axis, for different interaction range σ , 2-D interaction strength $g_2 = 0.9151$, in the regime $0 \leq L_z \leq 4N$.

IV. MANY-BODY QUANTUM CORRELATION

To further probe the systems we calculate the some other quantities of interest like von-Nuemann entropy degree of condensation and conditional probability density (CPD). Quantum correlation has been studied extensively to study the quantum nature of the systems [53, 54]. We calculated the SPRDM in Eq. (14), to calculate

the von-Neumann entropy defined in Eq. (19), Degree of condensation in Eq. (20) and CPD in Eq. (21).

A. QUANTUM ENTROPY

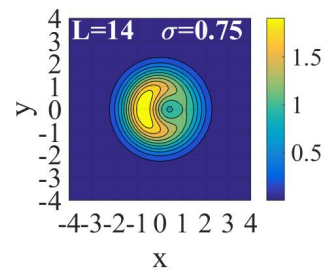
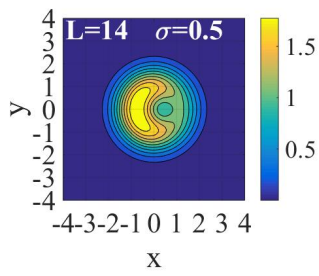
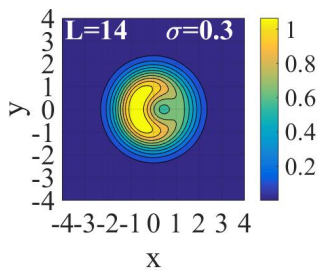
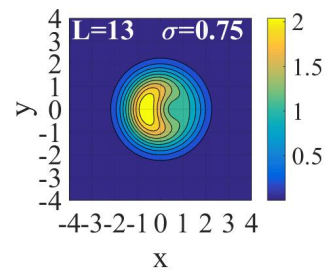
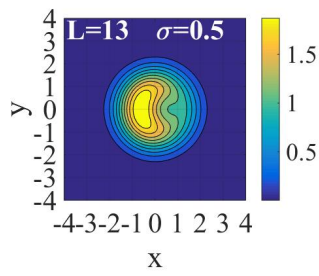
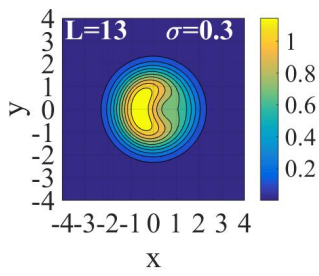
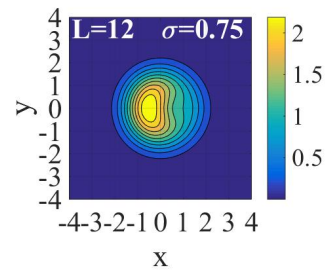
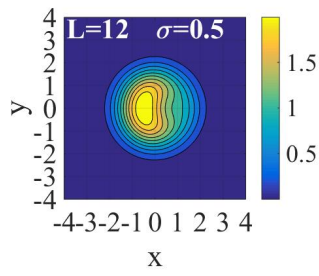
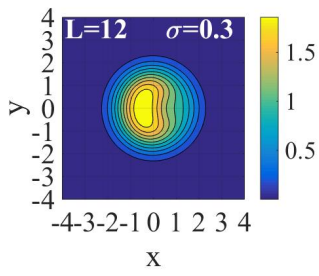
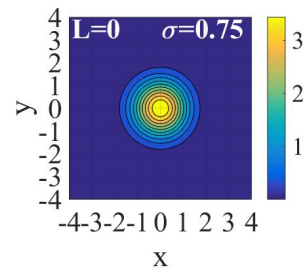
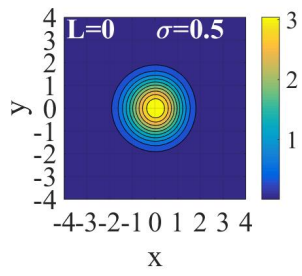
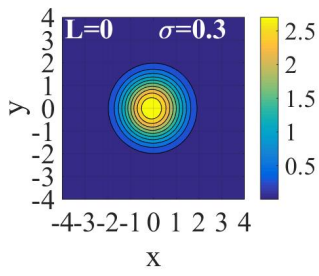
To study the quantum correlation of the many-body ground state, we calculated the von-Neumann entanglement entropy. It has been defined in different ways in thermodynamics, it has very well known form as $S = k_B \log \Omega$, where k_B is Boltzmann constant and Ω is canonical ensemble. In terms of reduced density matrix it is defined as [55–58]

$$S_1 = -\text{Tr}(\hat{\rho} \ln \hat{\rho}) \quad (18)$$

where, $\hat{\rho}$ is the single particle reduced density matrix obtained through the SPRDM in Eq. (14). In terms of the eigenvalues $\{\lambda_\mu\}$ of SPRMD calculated in the earlier section, the von-Neumann entanglement entropy explicitly becomes

$$S_1 = -\sum_{\mu} \lambda_{\mu} \ln \lambda_{\mu} \quad (19)$$

in the subspaces of total angular momentum L_z .



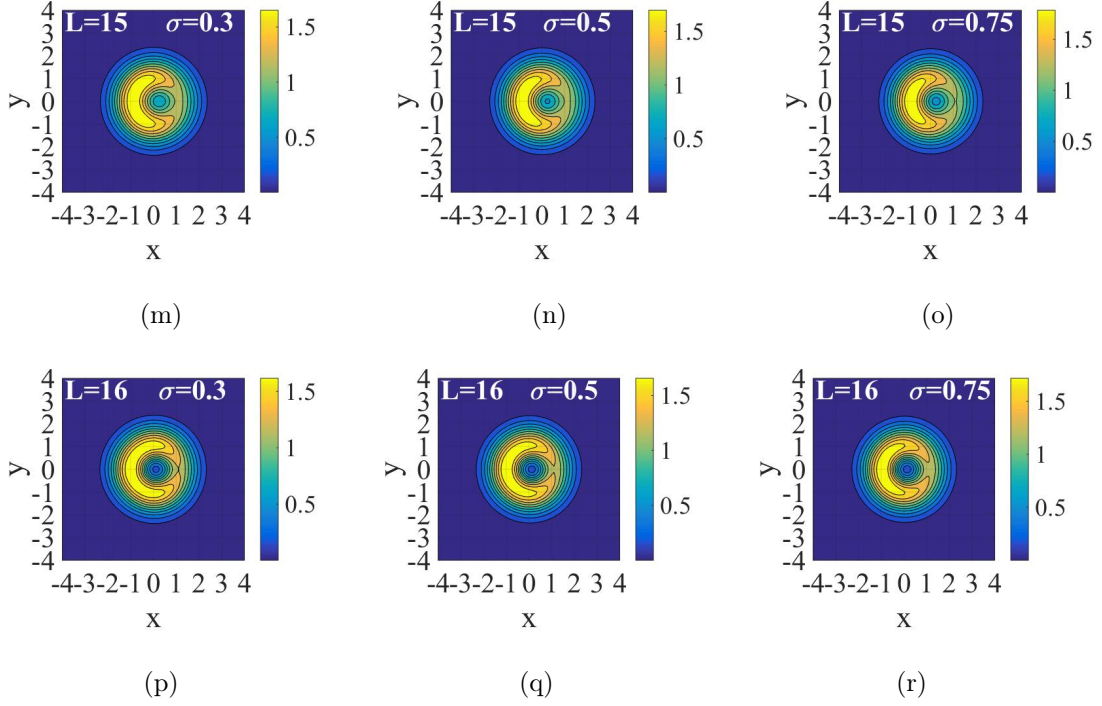


FIG. 10. (Color online) CPD contour plots for $N=16$ spin-0 bosons in subspace of total angular momentum $0 \leq L_z \leq N$ with interaction strength $g_2 = 0.9151$ and different interaction range parameter σ in the finite range smooth Gaussian potential in Eq. (2). These contour plots are iso-surface density profile viewed along the rotation axis- z . The reference point is chosen relatively large $\mathbf{r}_0 = (x_0, y_0) = (3, 0)$ in the units of a_\perp . Yellow represents the highest probability density region falling off to the least in blue region shown in the vertical color bar.

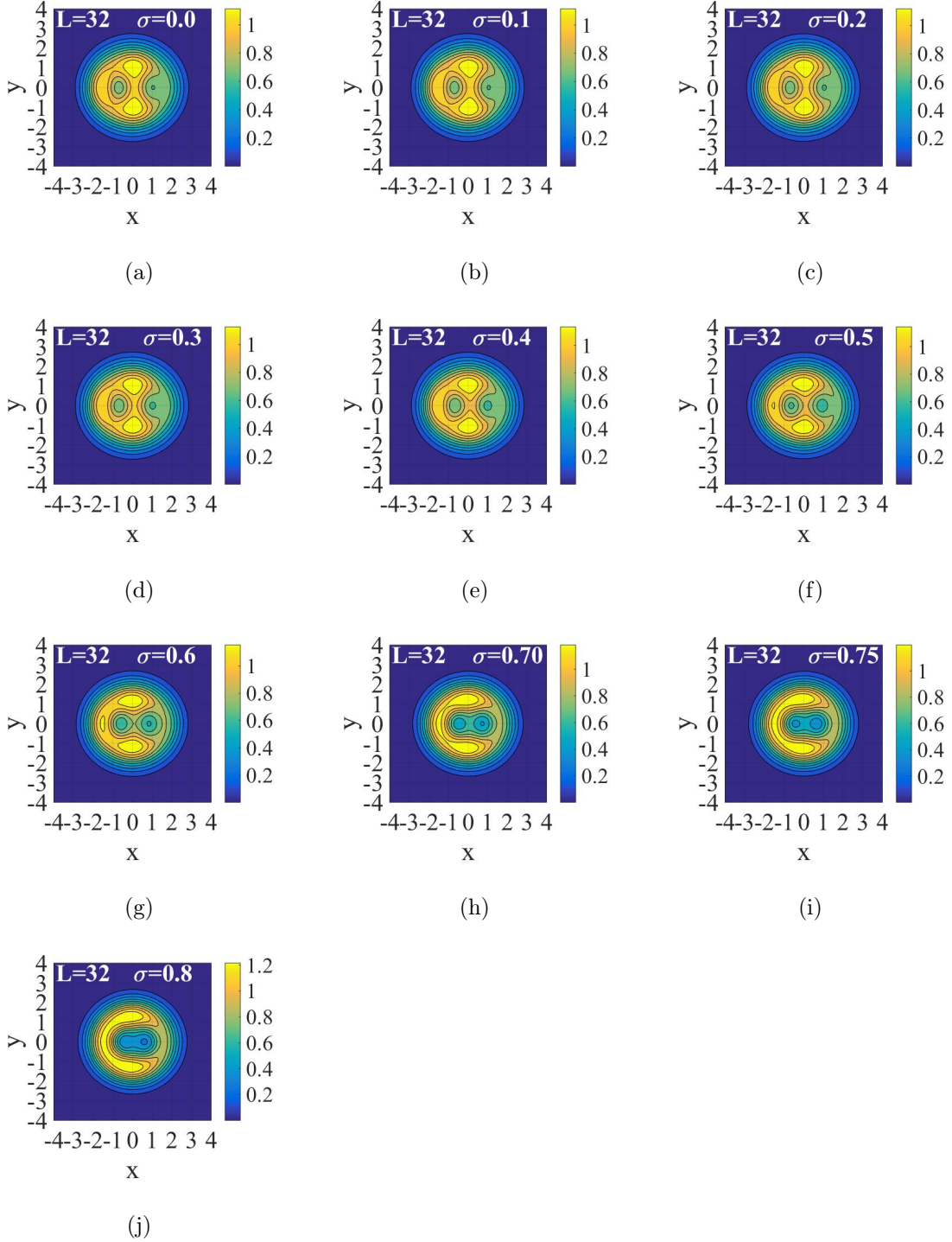


FIG. 11. (Color online) CPD contour plots for $N=16$ spin-0 bosons in subspace of total angular momentum $L_z = 32$ with interaction strength $g_2 = 0.9151$ and different interaction range parameter σ in the finite range smooth Gaussian potential in Eq. (2). These contour plots are iso-surface density profile viewed along the rotation axis- z . The reference point is chosen relatively large $\mathbf{r}_0 = (x_0, y_0) = (3, 0)$ in the units of a_\perp . Yellow represents the highest probability density region falling off to the least in blue region shown in the vertical color bar

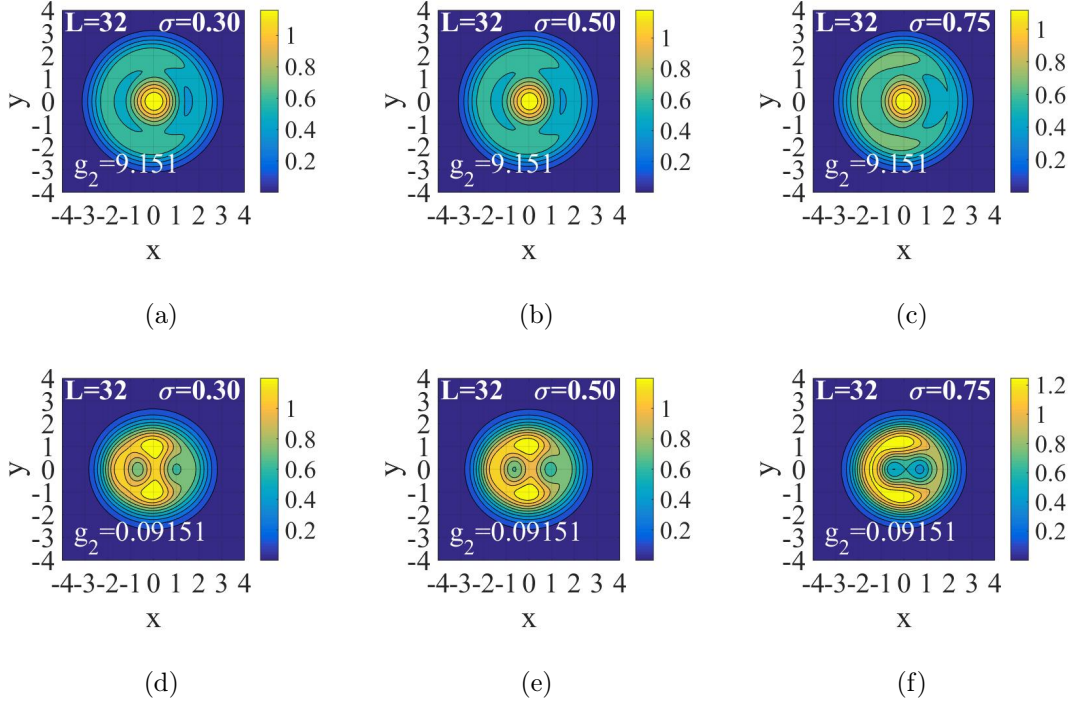


FIG. 12. (Color online) CPD contour plots for $N=16$ spin-0 bosons in subspace of total angular momentum $L_z = 32$ with different interaction strength g_2 and interaction range parameter σ in the finite range smooth Gaussian potential in Eq. (2). These contour plots are iso-surface density profile viewed along the rotation axis- z . The reference point is chosen relatively large $\mathbf{r}_0 = (x_0, y_0) = (3, 0)$ in the units of a_\perp . Patterns of vortex nucleation as function of g_2 . Yellow represents the highest probability density region falling off to the least in blue region shown in the vertical color bar.

B. DEGREE OF CONDENSATION

The degree of condensation is being calculated using the eigenvalues λ_μ , obtained from the one particle reduced density matrix (SPRDM) in Eq. (14).

$$C_d = \lambda_1 - \bar{\lambda} \quad (20)$$

where, $\bar{\lambda}_1 = \frac{1}{q-1} \sum_{\mu=2}^q \lambda_\mu$ is the arithmetic mean of the (N-1) eigenvalues. In the absence of condensation, the eigenstates are equally occupied, in such case the condensate would be zero[59]. In Fig. 3 and 4 we drawn two graphs to do a comparative study for von-Nueman entropy S_1 and degree of condensation C_d . For non rotating case i.e. $L_z = 0$, the entropy is minimum $S_1(\sigma) \rightarrow 0$ while the degree of condensation $C_d(\sigma) \rightarrow 1$ is maximum irrespective of interaction range σ , this is one of the signature of perfectly ordered state. As well for $L_z = 0$ the condensate fraction occupancy is maximum $\lambda_1 \rightarrow 1$ and all other $\lambda_{(\mu \geq 2)} \rightarrow 0$ in the ground state shown in Fig. 9. As L_z grows the condensate started depleting, more then one λ_μ acquires non-zero values hence S_1 increases. One of the effects of stirring the condensate gives rise to vortices, which start to appear at the critical angular velocity Ω_c , which is one of the most important signature of superfluidity will be discussed in details in coming sections. The S_1 is slowly increasing with the increase in L_z till $L_z = 11$ and then starts decreasing till the first vortex state $L_z = N$ appears has an oscillatory nature of varying amplitude throughout the entire range $0 \leq L_z \leq 4N$. There are minimum at every vortical state $L_z(\Omega_{\mathbf{c}_i})$. There are few local minima in S_1 appeared for the different interaction range σ against L_z are listed here,

$$L_z^{S_1}(\sigma = 0.30) = 0, \mathbf{16}, 19, 24, 26, \mathbf{28}, 30, 36, \mathbf{48}, 39, 44, \mathbf{52}, 55, \mathbf{60}.$$

$$L_z^{S_1}(\sigma = 0.50) = 0, \mathbf{16}, 19, 24, 26, \mathbf{28}, 30, \mathbf{36}, 39, 44, \mathbf{48}, \mathbf{52}, 55, \mathbf{60}.$$

$$L_z^{S_1}(\sigma = 0.75) = 0, \mathbf{16}, 19, 22, 24, 26, \mathbf{28}, \mathbf{30}, \mathbf{32}, \mathbf{36}, \mathbf{39}, 42, 45, \mathbf{48}, \mathbf{52}, 56, \mathbf{60}.$$

Fig. 1 belongs to these **bold** numbers correspond to the $L_z(\Omega_{\mathbf{c}_i}), i = 1, 2, \dots$. Therefore the von-Neumann entropy S_1 in Fig. 3 can also be studied in terms of stability-curve in Fig. 1. We can see clearly the finite range effects in the highly rotating regime, for example $S_1^{L_z=32}\{\sigma = 0.30\}(1.540) > S_1^{L_z=32}\{\sigma = 0.50\}(1.472) > S_1^{L_z=32}\{\sigma = 0.75\}(1.187)$. If we observe further, at $L_z = 22, 42, 50$ and 56 , a similar trend with the increase in interaction range occurs $S_1^{L_z=42}(\sigma = 0.30) > S_1^{L_z=42}(\sigma = 0.50) > S_1^{L_z=42}(\sigma = 0.75)$. We summarized that the $L_z = 32$ is a vortex state must have minimum S_1 to become a stable state which is only greatly favoured by the largest $\sigma = 0.75$. For non-vortical states at $L_z = 40$ and 50 the higher σ has minimum S_1 .

The another quantity of interest C_d defined in Eq. (20) can be defined in terms of von-Neumann entropy S_1 defined in Eq. (19) which is sensitive to the loss of macro-occupation. To ascertain the relation between C_d and S_1 , we compare the plots in Fig. 4 and 3. We can see that the effects shown by the both graphs are counter contrast in nature. For non rotating case i.e. $L_z = 0$, the degree of condensation C_d is maximum while the S_1 is minimum irrespective of interaction range σ . As rotation grows, C_d has peak and S_1 has a dip at $L_z^i(\Omega_{\mathbf{c}_i})$ as both shows competing effects. Minimum S_1 and maximum C_d corresponds maximum many-body quantum correlation among the particles and maximally condensate states. Dip in S_1 and peak in C_d can also be understood in the terms of vortex nucleation, first peak in C_d and the corresponding dip corresponds in S_1 to the first vortex state $N = L_z$ shown in iso-surface CPD plots in Fig 10(p), 10(q) and 10(r) with vorticity $m_1 = 1$. At $L_z = 32$, there is another dip in S_1 and peak in C_d corresponds to the higher $p = 2$ fold symmetrical vortex state with vorticity $m_1 = 2$ shown in the Fig. 14(e), 15(e) and 16(f) and $p = 5$ fold symmetrical vortices with vorticity $m_1 = 5$ are found at $L_z = 60$ corresponding the dip in S_1 and peak in C_d is shown here in Fig. 14(j), 15(j) and 16(l). The von-Neumann quantum entanglement entropy S_1 and degree of condensation C_d is listed

for the entire angular momentum state in range $0 \leq L_z \leq 4N$ in the Table VIII, ?? and ??, for different values of interaction range $\sigma = 0.30, 0.50$ and 0.75 respectively. These Tables contains few details columnwise, (i) orbital angular momentum L_z about the axis of rotation, (ii) ground state energy $E_0^{Lab}(L_z)$ in laboratory frame, (iii) critical angular y $\Omega_c(L_z^i)$, $i = 1, 2, 3, \dots$, discrete rotational symmetry, denoted by integer p , largest macroscopic occupation λ_1 (macroscopic eigenvalue) (λ_2, λ_3) (iv) corresponding single particle quantum numbers $n_1 m_1$ ($(n_2 m_2), (n_3 m_3)$). (v) degree of condensation C_d and the last (vi) the von-Neumann entropy S_1 . Further probing the system at second vortex state for angular momentum $L_z = 32(\sigma = 32)$, we plot Fig. 5, the von-Neumann entropy S_1 (degree of condensation C_d) decreases (increases) with the increase in the interaction range σ . In iso-surface CPD plots in Fig. 11 to observe the nucleation of vortices as the function of σ . The accumulation of probability density at the edge of vortices can be seen with increase in the interaction range σ . We compare the nucleation of vortex state around the second vortex in Fig. 17 and conclude this with the complete results in Tab. II.

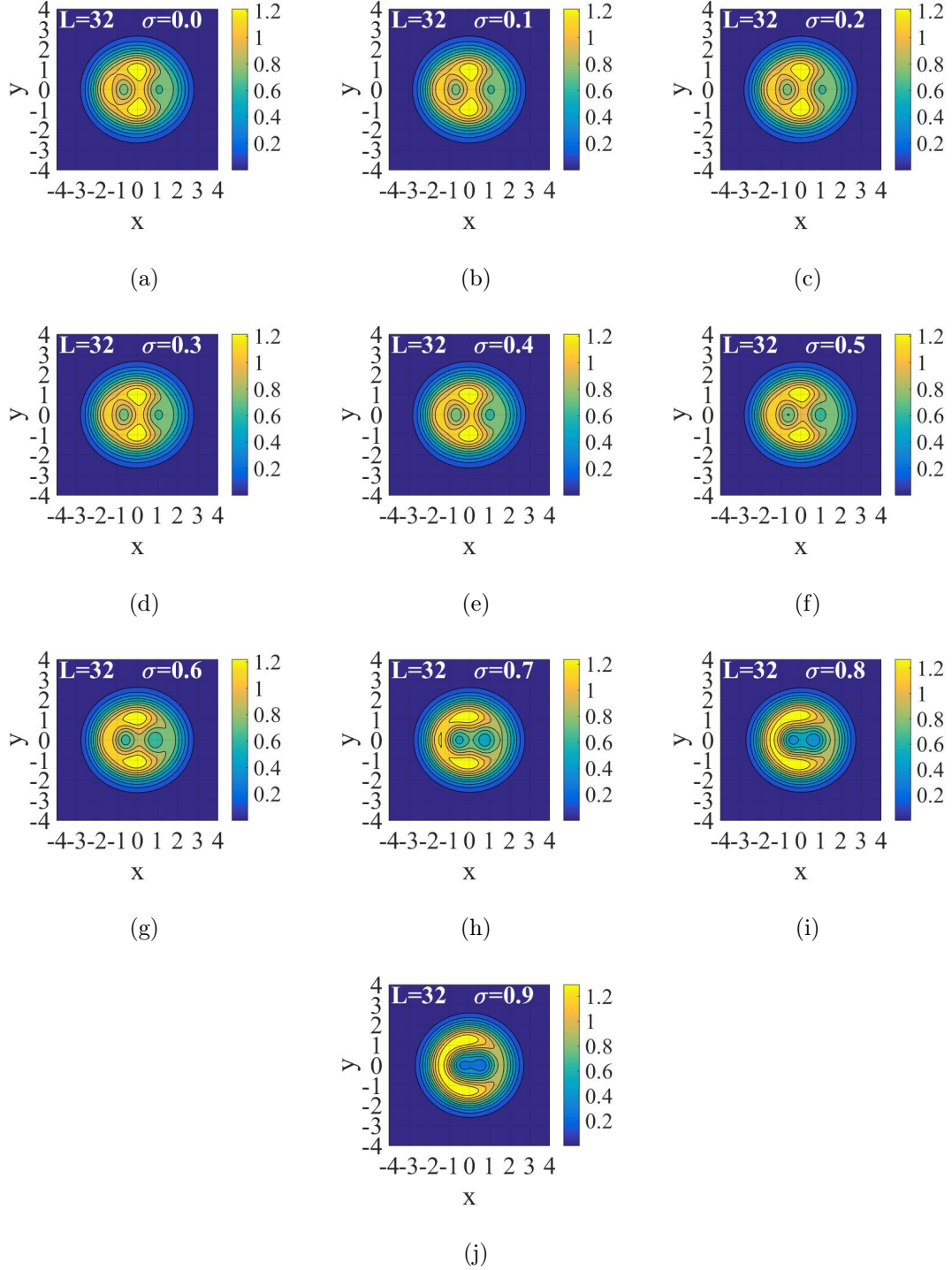


FIG. 13. (Color online) CPD contour plots for $N=16$ spin-0 bosons in subspace of total angular momentum $L_z = 32$ in LLL approximation $n_r = 0$ with interaction strength $g_2 = 0.9151$ and different interaction range parameter σ in the finite range smooth Gaussian potential in Eq. (2). These contour plots are iso-surface density profile viewed along the rotation axis- z . The reference point is chosen relatively large $\mathbf{r}_0 = (x_0, y_0) = (3, 0)$ in the units of a_\perp . Yellow represents the highest probability density region falling off to the least in blue region shown in the vertical color bar

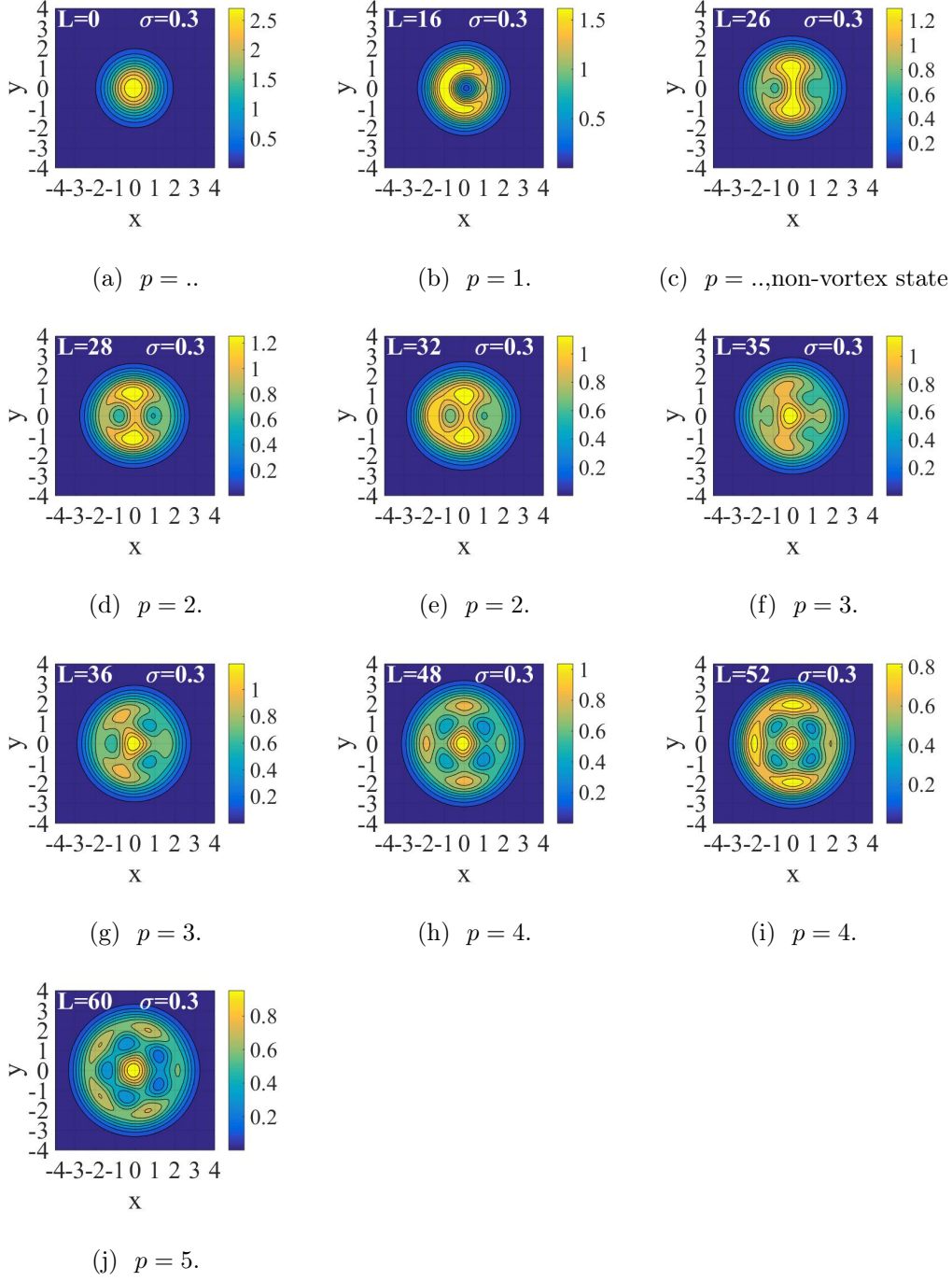


FIG. 14. CPD contour plots for $N=16$ spin-0 bosons in subspace of total angular momentum $0 \leq L_z \leq 4N$ with interaction strength $g_2 = 0.9151$ and interaction range parameter $\sigma = 0.30$ in the finite range smooth Gaussian potential in Eq. (2). These contour plots are iso-surface density profile viewed along the rotation axis- z with p -fold symmetry ($p = 1, 2, 3, 4, ..$). The reference point is chosen relatively large $\mathbf{r}_0 = (x_0, y_0) = (3, 0)$ in the units of a_\perp for (14(a)-14(e)) and at (1.5,0) for (14(f)-14(j)). Yellow represents the highest probability density region falling off to the least in blue region shown in the vertical color bar.

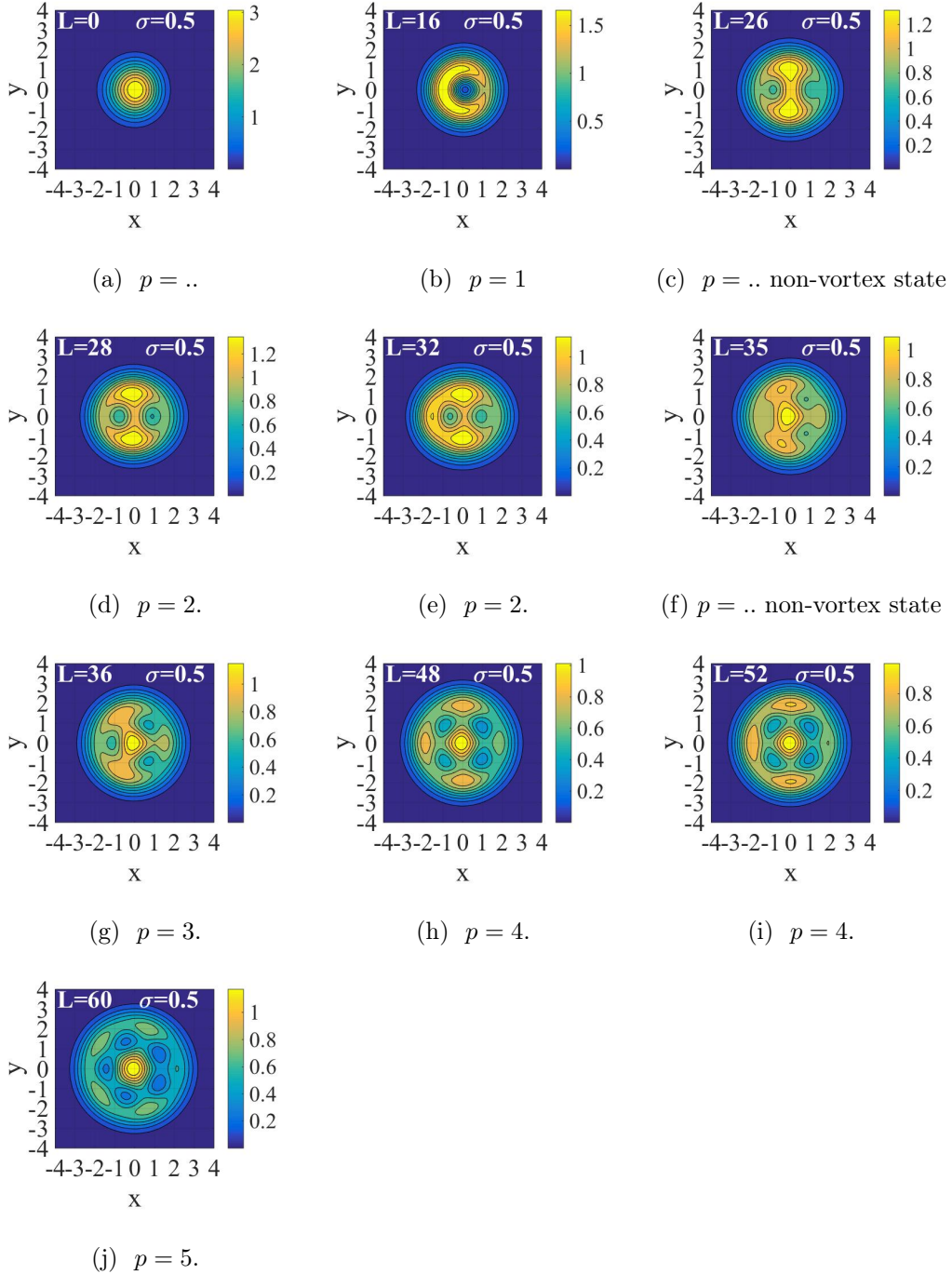


FIG. 15. (Color online) CPD contour plots for $N=16$ spin-0 bosons in subspace of total angular momentum $0 \leq L_z \leq 4N$ with interaction strength $g_2 = 0.9151$ and interaction range parameter $\sigma = 0.50$ in the finite range³⁹ smooth Gaussian potential in Eq. (2). These contour plots are iso-surface density profile viewed along the rotation axis- z with p -fold symmetry ($p = 1, 2, 3, 4, ..$). The reference point is chosen relatively large $\mathbf{r}_0 = (x_0, y_0) = (3, 0)$ in the units of a_\perp for (15(a)-15(e)) and at $(1.5, 0)$ for (15(f)-15(j)). Yellow represents the highest probability density region falling off to the least in blue region shown in the vertical color bar.

	$n_r = 0$			$n_r = 1$		
L_z	$E_0^{lab}(\sigma = 0.3)$	$E_0^{lab}(\sigma = 0.5)$	$E_0^{lab}(\sigma = 0.75)$	$E_0^{lab}(\sigma = 0.3)$	$E_0^{lab}(\sigma = 0.5)$	$E_0^{lab}(\sigma = 0.75)$
0	46.864	46.359	45.368	49.132	47.871	46.080
16	59.252	58.904	58.463	59.613	59.164	58.634
28	70.133	69.867	69.560	70.310	69.988	69.637
32	73.831	73.593	73.318	73.950	73.674	73.375
48	88.890	88.738	88.602	88.956	88.781	88.630
60	100.635	100.487	100.358	100.650	100.495	100.362
64	104.613	104.464	104.315	104.637	104.480	104.326

TABLE I. In this Table we note the ground state energy $E_0(\sigma)$ for Landau level approximation($n_r = 0$) and for beyond Lowest level approximation($(n_r = 1)$) in the sub-space of total angular momentum L_z .

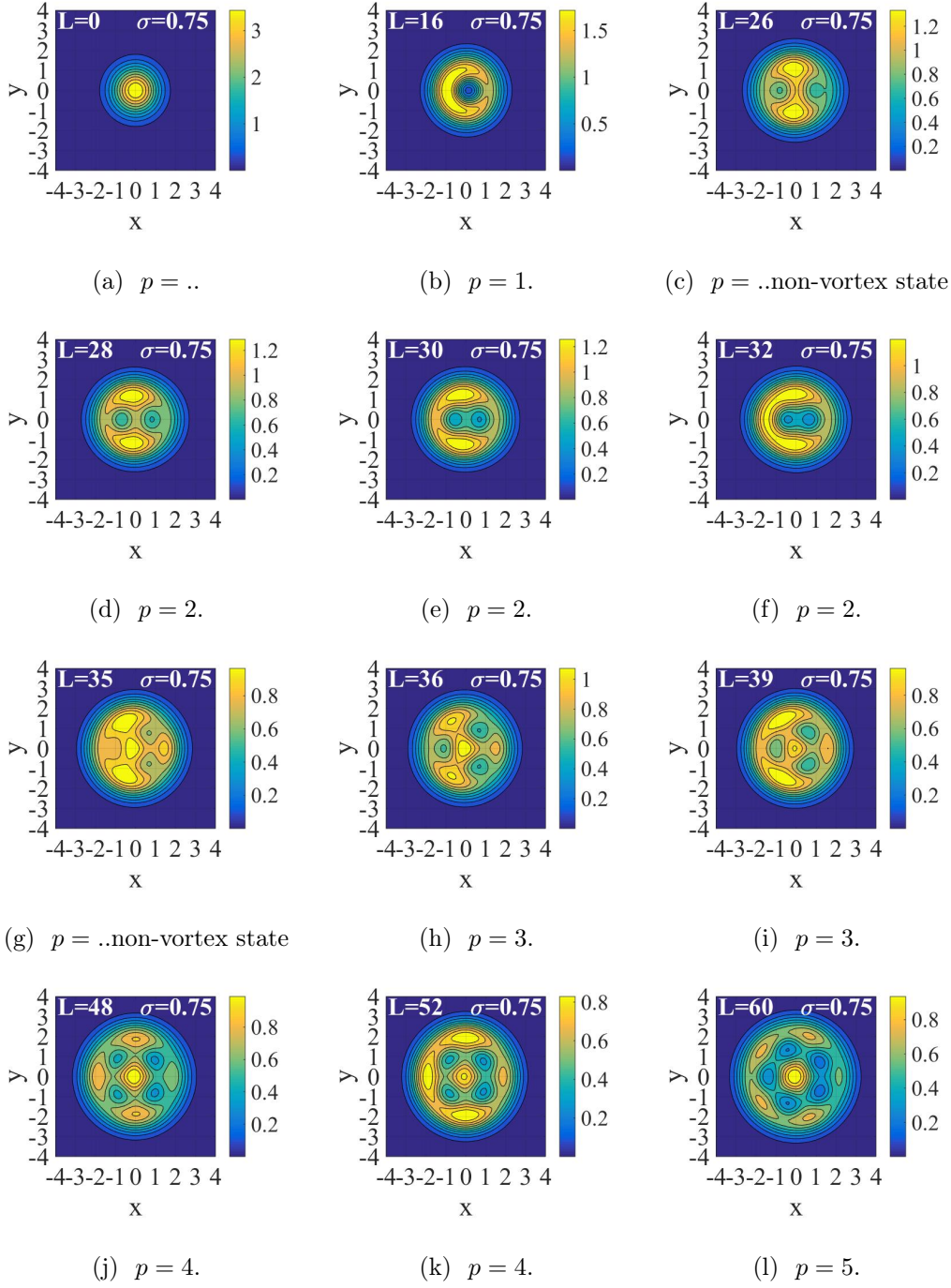


FIG. 16. CPD contour plots for $N=16$ spin-0 bosons in subspace of total angular momentum $0 \leq L_z \leq 4N$ with interaction strength $g_2 = 0.9151$ and interaction range parameter $\sigma = 0.75$ in the finite range smooth-Gaussian potential in Eq. (2). These contour plots are iso-surface density profile viewed along the rotation axis- z with p -fold symmetry ($p = 1, 2, 3, 4, ..$). The reference point is chosen relatively large $\mathbf{r}_0 = (x_0, y_0) = (3, 0)$ in the units of a_\perp for (16(a)-16(f)) and at (1.5,0) for (16(g)-16(l)). Yellow represents the highest probability density region falling off to the least in blue region shown in the vertical color bar.

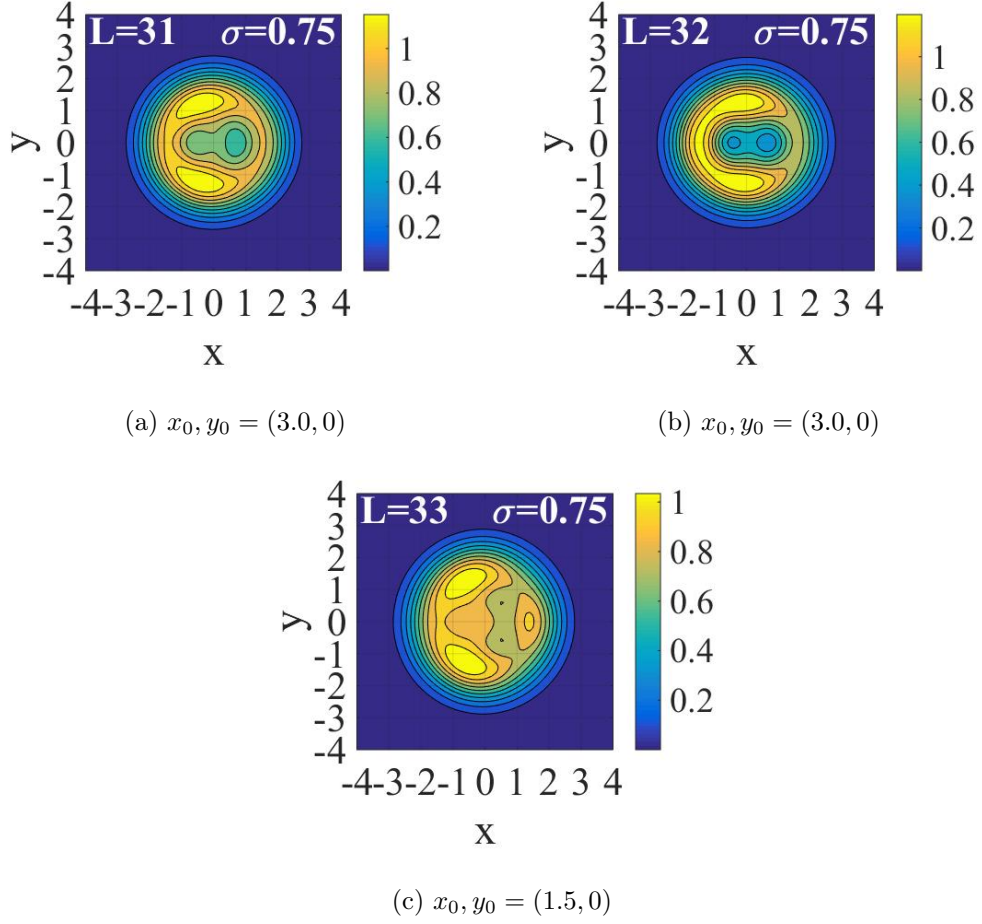


FIG. 17. (Color online) For $N=16$ bosons, CPD isosurface contour plots for different total orbital angular momentum L_z for a fixed interaction range $\sigma = 0.75$ and strength $g_2 = 0.9151$. The reference point is chosen at $\mathbf{r}_0 = (3, 0)$ in the units of a_\perp . Probability density strength is shown in vertical color bar.

C. CONDITIONAL PROBABILITY DENSITY

To further probe the ground state property of weakly interaction bose gas, we calculate the Conditional Probability Density (CPDs). The CPDs is the measures of an intrinsic density distribution of bosons which makes it a experimental observable quantity over the circularly symmetric density distribution. This become an important tool to measure the boson density in the condensed bose gas where the circular symmetry is broken spontaneously. It is noted that CPDs is also used for measure of electron correlations in doubly excited helium like atoms [60, 61] and in quantum dot to study the formation of Wigner molecules[62, 63]. The CPDs $\rho(\mathbf{r}, \mathbf{r}_0)$ is defined as the probability of finding one boson at position \mathbf{r} given that the other particle is at \mathbf{r}_0 is mathematically defined as. [24, 64].

$$\rho(\mathbf{r}, \mathbf{r}_0) = \frac{\sum_{i \neq j} \langle \Psi | \delta(\mathbf{r} - \mathbf{r}_i) \delta(\mathbf{r}_0 - \mathbf{r}_j) | \Psi \rangle}{(N - 1) \sum_j \langle \Psi | \delta(\mathbf{r}_0 - \mathbf{r}_j) | \Psi \rangle} \quad (21)$$

where, $|\Psi\rangle$ represent the ground state single particle wave function obtained from the exact diagonalization and \mathbf{r}_0 is the reference point in the x-y plane. Choice of reference $\mathbf{r}_0 = (x_0, y_0)$ (in units of a_\perp) is chosen purposefully, for smaller orbital angular momentum $0 \leq L_z \leq 2N$, is given a significantly large value so that the symmetry breaking should be visible i.e. $(3, 0)$ and for $2N \leq L_z \leq 4N$, as condensate starts depletion and CPD contour starts shrinking inward hence the choice of reference is reduced to $(1.5, 0)$, for large number of particles, CPD contour becomes independent of \mathbf{r}_0 [14] however [66] disagree with this.

1. SINGLE VORTEX STATE

In this section, we are confined in orbital angular momentum range $0 \leq L_z < N$. In Fig. 10, We have taken $L_z = 0, 12, 13, 14, 15$ and 16 for different interaction range $\sigma = 0.30, 0.50$ and 0.75 have observed that the reference point plays an important role in the view-point of CPD symmetry. The feature is not visible unless the reference is not chosen significantly larger. The non-rotating orbital angular momentum state $L_z = 0$ has a Gaussian symmetry for all σ despite increase in the probability density strength with increase in σ from 2.5 to 3.0 (shown in vertical bar) in Fig. 10(a), 10(b) and 10(c). There is decrease in probability density strength with increase in the angular momentum as the condensate deplete with increasing in L_z . With the increase in L_z the Gaussian symmetry has diminished and envelope has started moving inward from the periphery, can be viewed in Fig. 10(d), 10(e) and 10(f). The observed broken symmetry starts emerging from $l_z(\sigma = 0.30, 0.50, 0.75) = 0.75 = 12/16$, $0.81 = 13/16$ unless and is not visible until the reference point \mathbf{r}_0 is not chosen relatively large, in our case $(3, 0)$. The symmetry breaking first occurred for the large interaction range $\sigma = 0.75$ followed by the smaller $\sigma = 0.30$ can be seen at $l_z(\sigma = 0.30, 0.50, 0.75) = 0.88 = 14/16$ where the first signature of vortex nucleation appears onwards in Fig. 10(j), 10(k) and 10(l). The complete central vortex appears at $l_z = 1$, in Fig. 10(p), 10(q) and 10(r) corresponding to first critical angular velocity $\Omega_{\mathbf{c}_1}$, shown in the Fig. 1, minimum in von-Neumann entropy S_1 shown in Fig. 3 and peak in the degree of condensation C_d shown in the Fig. 4 as well in condensate fraction λ_1 in Fig. 6, 7 and 8. The quantized vortex has same value (vorticity) $m_1 = 1$ for the quantum number $n = 1, 3$, shown in Table III, IV and V. In conclusion we say that the larger interaction range σ facilitates the nucleation of vortex. Emergence of single vortex state is studied by [65] for δ in LLL approximation for harmonic trap.

2. MULTIPLE VORTEX STATE

We presented the study of single vortex state $N = L_z$ in the earlier section for all three interaction ranges in CPDs contour in Fig. 10 now we are going to present the study for higher vortices in the orbital angular momentum range $N \geq L_z \leq 4N$ with interaction range parameter σ as we observed that the emergence of profiles first appears for higher σ . Interaction range σ is an important agent to play with in order to understand the many-body effects of Bose-Einstein condensate through vortices nucleation. $N = 16$ is sufficient number of particles to study the many-body effect on higher vortices to study the Bose-Einstein condensation for different interaction ranges.

As angular momentum increased beyond $L_z = N$ some additional vortices started to appear and arranged themselves into the regular lattice patterns as shown in Fig. 14, 15 and 16 includes some unstable stable vortices for all three interaction range $\sigma = 0.30, 0.50$ and 0.75 . The orbital angular momentum $L_z = 26$ is unstable state with single vortex for all values of σ shown in Fig. 14(c), 15(c) and 16(c) referring to the stability curve shown in the Fig. 1 corresponding dip in von-Neumann entropy S_1 shown in Fig. 3, peak in the degree of condensation C_d as shown in the Fig. 4 and in condensate fraction λ_1 in Fig. 9. The second stable vortex state ($L_z = 28$), appears at the critical velocity Ω_{c_2} , has $p = 2$ fold symmetry. The quantized vortex has same value (vorticity) $m_1 = 2$ for the quantum number $n = 2, 4$, shown in Table III, IV and V a quantum jump, and the isosurface CPD contour in the Fig. 14(d), 15(d) and 16(d). For the $\sigma = 0.75$, in the stability curve Fig 1, appears at the orbital angular momentum $L_z = 30$ is stable vortex state which is absent for $\sigma = 0.30$ and 0.50 , further a peak can be clearly seen in the condensate fraction λ_1 a dip in the von-Neuman entropy, peak in the degree of condensation C_d and the 2-fold symmetry isosurface in CPDs contour shown in Fig. 16(e), next $p = 2$ fold symmetrical vortices

are set to be at the orbital angular momentum $L_z = 32$ for all three interaction range $\sigma = 0.30, 0.50$ and 0.75 as shown in Fig. 14(e), 15(e) and 16(f). At this point we need to check the finite range effects, we observed that with increase in the parameter σ condensate fraction and degree of condensation has been increased as shown in Fig. 9 and 4 and corresponding decrease in the von-Neumann entropy S_1 is also reported in Fig. 3. We plot the CPDs for $0 \leq \sigma \leq 0.80$ to further focus the change of state with the change of σ here are few more CPDs contour plots shown here in Fig. 11.

In Fig 17 for a fixed interaction range $\sigma = 0.75$ and in the subspace of total angular $31 \geq L_z \leq 33$ the acculumation of particles density at the core of vortices has been reported in Fig. 17(b). Here in Fig. 11, we study the differences in isosurface CPD contour. With the increase in the interaction range σ , emergence of stronger and equall depth vortices peak and the formation of hill of higher density around the vortices. One more thing to record is that, with the increase in σ , nucleated vortices are going through signature change despite being the stable state (not sure for $\sigma = 0.0, 0.1, 0.2, 0.4, 0.60, 0.70$ and 0.80). Complete results are written in the Table. II

For fast rotating case, in the orbital angular momentum range $2N > L_z \leq 4N$, higher p= 3, 4, 5...-fold symmetry started to emerge. we have triangular lattice for $L_z = 35$, 14(f) and $L_z = 36$, 14(g), 15(g) and 16(h). The vortices have arranged in a regular arrangements of Abrikosov lattices [31, 32]. Square vortic lattices are shown in Fig. 14(h), 14(i), 15(h), 15(i) and 16(j), 16(k) and pentagonal vortic lattices 14(j), 15(j) and 16(l) appears for the orbital angular momentum $L_z = 48, 52$ and 60 for all three interaction range parameter σ in accordance with the stability graph in Fig. 1. For interaction range $\sigma = 0.75$ and $L_z = 35$ is not the critical state in contrast to other $\sigma = 0.30$ and 0.50 we do this plot for the comparative study.

TABLE II. For $N=16$ bosons, interacting via finite range Gaussian potential in Eq. (1) with interaction strength $g_2 = 0.9151$ and different interaction range σ . with their vorticity (m_μ) ($\mu = 1, 2, 3$) are reported from SPRDM in Eq. (14) in given subspaces of the total angular momentum $L_z = 32$ along with von-Neumann entropy S_1 and ground state energy $E_0^{Lab}(L_z)$. Here the state has been changed with the increase in σ .

σ	n_1, m_1	n_2, m_2	n_3, m_3	S_1	$E_0^{Lab}(L_z)$
0.00	2,2	0,0	4,4	1.56	74.04561
0.10	2,2	0,0	4,4	1.56	74.01746
0.20	2,2	0,0	4,4	1.55	73.94022
0.30	2,2	0,0	4,4	1.54	73.83171
0.40	2,2	0,0	4,4	1.52	73.71143
0.50	2,2	0,0	4,4	1.47	73.59262
0.60	2,2	0,0	4,4	1.39	73.47973
0.70	2,2	0,0	3,3	1.26	73.37109
0.75	2,2	3,3	1,1	1.19	73.31758
0.80	2,2	1,1	3,3	1.11	73.26460

V. SUMMARY AND CONCLUSION

For a system of $N=16$ spin-0 bosons interacting via a finite range normalized Gaussian potential in an harmonic trap. Our scheme suggests that for many-body system in finite range has explicit dependency of the range σ and strength g_2 . We explicitly shown that the critical angular velocity $\{\Omega_{c_i}, i = 1, 2, \dots\}$ increases with increase in interaction range. Apart from this, length and height of plateaus also depends on the finite range σ for a given parameters shown in the stability graph in Fig.1. In the Condensate fraction λ_1 , the finite range effects are dominant in the higher angular momentum regime, $N < L_z < 4N$. Fig.9 as well as the von-Neumann entropy and degree of condensation too shows variation for higher L_z as shown in Fig. 3 and 4 with this we conclude that the vortex entry takes place first for higher σ followed by the smaller σ .

TABLE III. For $N=16$ bosons, The many-body ground state energies in Lab frame $E_0^{lab}(L_z^i)$, interacting via finite range Gaussian potential in Eq. (1) with interaction strength $g_2 = 0.9151$ and interaction range $\sigma = 0.30$. Three largest macroscopic eigenvalues $\lambda_1 > \lambda_{(\mu \geq 2)}$, weight $|c_{n,m_1}^1|^2$ of the corresponding states with their quantum numbers (n, m_1) are reported from SPRDM in Eq. (14) respectively along with critical angular velocity $\Omega_{\mathbf{c}}(L_z^i)$, $i = 1, 2, 3, \dots$, in given subspaces of the total angular momentum L_z^i .

L_z^i	$E_0^{lab}(L_z^i)$	$\Omega_{\mathbf{c}}(L_z^i)$	(n, m_1)	$ c_{n,m_1}^1 ^2$	λ_1
0	46.86428	0.0000	0, 0	0.97593	0.98949
			2, 0	0.21809	
16	59.25225	0.77425	1, 1	0.99542	0.87484
			3, 1	0.09558	
28	70.13310	0.90674	2, 2	0.99684	0.61063
			4, 2	0.07941	
32	73.83171	0.92465	2, 2	0.99814	0.43495
			4, 2	0.06089	
35	76.62143	0.92990	3, 3	0.99786	0.32727
			5, 3	0.06540	
36	77.55398	0.93255	3, 3	0.99793	0.48498
			5, 3	0.06429	
48	88.89032	0.94469	4, 4	0.99900	0.48443
			6, 4	0.04476	
52	92.79163	0.97533	4, 4	0.99916	0.54632
			6, 4	0.04103	
60	100.63525	0.98045	5, 5	1.0000	0.49277

TABLE IV. For N=16 bosons, The many-body ground state energies in Lab frame $E_0^{lab}(L_z^i)$, interacting via finite range Gaussian potential in Eq. (1) with interaction strength $g_2 = 0.9151$ and interaction range $\sigma = 0.50$. Three largest macroscopic eigenvalues $\lambda_1 > \lambda_{(\mu \geq 2)}$, weight $|c_{n,m_1}^1|^2$ of the corresponding states with their quantum numbers (n, m_1) are reported from SPRDM in Eq. (14) respectively along with critical angular velocity $\Omega_{\mathbf{c}}(L_z^i)$, $i = 1, 2, 3, \dots$, in given subspaces of the total angular momentum L_z^i .

L_z^i	$E_0^{lab}(L_z^i)$	$\Omega_{\mathbf{c}}(L_z^i)$	(n, m_1)	$ c_{n,m_1}^1 ^2$	λ_1
0	46.35902	0.0000	0, 0	0.98153	0.99292
			2, 0	0.19131	
16	58.90377	0.78405	1, 1	0.99650	0.87949
			3, 1	0.08360	
28	69.86716	0.91362	2, 2	0.99773	0.61129
			4, 2	0.06737	
32	73.59262	0.93136	2, 2	0.99866	0.48124
			4, 2	0.05178	
36	77.34967	0.93926	3, 3	0.99846	0.48347
			5, 3	0.05554	
48	88.73774	0.94901	4, 4	0.99923	0.47930
			6, 4	0.03931	
52	92.64065	0.97573	4, 4	0.99935	0.54190
			2, 0	0.02151	
60	102.50076	0.98079	6, 6	1.0000	0.40369

TABLE V. For N=16 bosons, The many-body ground state energies in Lab frame $E_0^{lab}(L_z^i)$, interacting via finite range Gaussian potential in Eq. (1) with interaction strength $g_2 = 0.9151$ and interaction range $\sigma = 0.75$. Three largest macroscopic eigenvalues $\lambda_1 > \lambda_{(\mu \geq 2)}$, weight $|c_{n,m_1}^1|^2$ of the corresponding states with their quantum numbers (n, m_1) are reported from SPRDM in Eq. (14) respectively along with critical angular velocity $\Omega_{\mathbf{c}}(L_z^i)$, $i = 1, 2, 3, \dots$, in given subspaces of the total angular momentum L_z^i .

L_z^i	$E_0^{lab}(L_z^i)$	$\Omega_{\mathbf{c}}(L_z^i)$	(n, m_1)	$ c_{n,m_1}^1 ^2$	λ_1
0	45.36785	0.0000	0, 0	0.98978	0.99664
			2, 0	0.14263	
16	58.46294	0.81844	1, 1	0.99650	0.87949
			3, 1	0.08360	
28	69.55952	0.92471	2, 2	0.99854	0.62821
			4, 2	0.05405	
30	71.43247	0.93648	2, 2	0.99886	0.67711
			4, 2	0.04779	
32	73.31758	0.94256	2, 2	0.99912	0.63923
			4, 2	0.04202	
36	77.12801	0.95262	3, 3	0.99894	0.50812
			5, 3	0.04597	
39	79.98856	0.95352	3, 3	0.99914	0.53684
			5, 3	0.04148	
48	88.60174	0.95702	4, 4	0.99942	0.46760
			6, 4	0.03406	
52	93.51604	0.97464	4, 4	0.99960	0.32485
			6, 4	0.02834	
60	100.35792	0.98220	5, 5	1.0000	0.50544

TABLE VI: Many-body ground state energies in Lab frame, E_0^{lab} , for $N=16$ bosons interacting via finite range Gaussian potential given in Eq. (1), with interaction strength $g_2 = 0.9151$ and interaction range $\sigma = 0.30$. The three largest macroscopic eigenvalues $\lambda_1 > \lambda_2 > \lambda_3$ of the SPRDM, corresponding single particle quantum numbers (n_1, m_1) , (n_2, m_2) and (n_3, m_3) respectively, degree of condensation C_d and von-Neumann entropy S_1 are calculated from SPRDM in Eq. (14) along with critical angular velocity Ω_c and p -fold symmetry in the total angular momentum space ranging from $0 \leq L_z \leq 4N$ are noted below in beyond LLL $n_r = 1$.

L_z	$E_0^{Lab}(L_z)$	Ω_c	p	(n_1, m_1)	λ_1	(n_2, m_2)	λ_2	(n_3, m_3)	λ_3	C_d	S_1
0	46.86428	0.0	-	0,0	0.98949	1,-1	0.00378	1,1	0.00378	0.98833	0.07430
1	47.87008			0,0	0.92247	1,1	0.06723	1,-1	0.00643	0.91385	0.31638
2	48.63374			0,0	0.91733	2,2	0.05309	1,1	0.02279	0.90814	0.36496
3	49.32981			0,0	0.91477	3,3	0.05037	1,1	0.01778	0.90530	0.39136
4	50.25820			0,0	0.83190	1,1	0.09654	2,2	0.03397	0.81322	0.64360
5	51.02044			0,0	0.81554	1,1	0.07699	2,2	0.06578	0.79505	0.69920
6	51.76595			0,0	0.80862	3,3	0.07690	2,2	0.07077	0.78736	0.71579
7	52.59151			0,0	0.70849	1,1	0.17101	2,2	0.07419	0.67610	0.90531
8	53.34973			0,0	0.66720	1,1	0.19594	2,2	0.08829	0.63022	0.97283
9	54.10657			0,0	0.61417	1,1	0.24315	2,2	0.09162	0.57131	1.03552
10	54.86196			0,0	0.54235	1,1	0.31429	2,2	0.10388	0.49151	1.07763
11	55.60626			0,0	0.47917	1,1	0.37575	2,2	0.10950	0.42130	1.09831
12	56.34683			1,1	0.44883	0,0	0.40950	2,2	0.11146	0.38759	1.09055

13	57.08395		1,1	0.53212	0,0	0.33439	2,2	0.10924	0.48013	1.04701	
14	57.81826		1,1	0.62887	0,0	0.25247	2,2	0.10044	0.58764	0.95374	
15	58.54967		1,1	0.74481	0,0	0.16083	2,2	0.08223	0.71646	0.78072	
16	59.25225	0.77425	-	1,1	0.87484	0,0	0.06268	2,2	0.05460	0.86347	0.49646
17	60.25409		1,1	0.72000	2,2	0.14957	0,0	0.11366	0.69455	0.85252	
18	61.23338		1,1	0.62690	2,2	0.19541	0,0	0.14181	0.59298	1.04460	
19	62.05475		1,1	0.73381	2,2	0.10344	0,0	0.09326	0.70961	0.92369	
20	63.00573		1,1	0.54544	2,2	0.22910	0,0	0.15422	0.50412	1.20600	
21	63.93098		1,1	0.37760	2,2	0.33382	0,0	0.21138	0.32102	1.32639	
22	64.79399		2,2	0.36431	1,1	0.30116	0,0	0.23872	0.30652	1.36787	
23	65.70191		2,2	0.40268	1,1	0.27154	0,0	0.22220	0.34837	1.37355	
24	66.54940		2,2	0.53143	0,0	0.28750	1,1	0.08470	0.48884	1.19590	
25	67.49024		2,2	0.46150	0,0	0.21617	1,1	0.18994	0.41254	1.37520	
26	68.31986		2,2	0.58021	0,0	0.24529	4,4	0.07453	0.54205	1.15945	
27	69.31222		2,2	0.50609	0,0	0.19009	1,1	0.14434	0.46119	1.34971	
28	70.13310	0.90674	2	2,2	0.61063	0,0	0.20011	4,4	0.08265	0.57524	1.15051
29	71.16949		2,2	0.47328	0,0	0.19354	3,3	0.17233	0.42540	1.38655	
30	71.99933		2,2	0.61755	0,0	0.16475	4,4	0.10182	0.58278	1.16531	
31	73.03732		2,2	0.42735	3,3	0.20508	0,0	0.19018	0.37529	1.44184	
32	73.83171	0.92465	2	2,2	0.43495	0,0	0.19058	4,4	0.14261	0.38358	1.53990
33	74.77374		3,3	0.26996	0,0	0.24653	2,2	0.22551	0.20360	1.67774	
34	75.70208		3,3	0.26981	2,2	0.23826	0,0	0.23264	0.20343	1.66348	
35	76.62143	0.92991	3	3,3	0.32727	0,0	0.24476	2,2	0.18294	0.26611	1.62796
36	77.55398	0.93255	3	3,3	0.48498	0,0	0.24302	2,2	0.10486	0.43816	1.41080
37	78.52752		3,3	0.28141	0,0	0.21992	2,2	0.20067	0.21608	1.70601	

38	79.45758		3,3	0.36911	0,0	0.21714	2,2	0.15734	0.31176	1.61093	
39	80.39032		3,3	0.47656	0,0	0.20374	4,4	0.12276	0.42898	1.46202	
40	81.37679		0,0	0.24484	4,4	0.22016	3,3	0.19725	0.17619	1.72851	
41	82.34432		3,3	0.32571	0,0	0.19444	4,4	0.15778	0.26441	1.67173	
42	83.28308		3,3	0.35277	0,0	0.19483	4,4	0.16750	0.29393	1.64412	
43	84.23940		4,4	0.33911	0,0	0.24764	3,3	0.16590	0.27903	1.61433	
44	85.17724		4,4	0.44093	0,0	0.26281	5,5	0.10992	0.39011	1.46003	
45	86.19175		4,4	0.25767	0,0	0.24947	5,5	0.23945	0.19018	1.65250	
46	87.16767		4,4	0.28202	0,0	0.19966	5,5	0.19827	0.21675	1.68982	
47	88.09247		4,4	0.37420	0,0	0.21216	5,5	0.16681	0.31731	1.57529	
48	88.89032	0.94469	4	4,4	0.48443	0,0	0.22052	3,3	0.10773	0.43757	1.48350
49	89.92046		4,4	0.32123	0,0	0.21793	5,5	0.17497	0.25953	1.69896	
50	90.90461		4,4	0.21761	0,0	0.20342	3,3	0.20182	0.14648	1.83417	
51	91.86018		4,4	0.28196	3,3	0.21103	0,0	0.18267	0.21668	1.76550	
52	92.79163	0.97533	4	4,4	0.54632	0,0	0.17165	3,3	0.09413	0.50507	1.40655
53	93.81503		4,4	0.29268	5,5	0.19396	0,0	0.17741	0.22837	1.75579	
54	94.79663		5,5	0.23017	0,0	0.21764	4,4	0.19550	0.16018	1.79180	
55	95.76346		5,5	0.40131	0,0	0.24870	6,6	0.13557	0.34689	1.59887	
56	96.74138		6,6	0.36293	1,1	0.22038	0,0	0.11831	0.30501	1.72438	
57	97.74751		6,6	0.31343	5,5	0.17286	0,0	0.16517849	0.25101	1.81372	
58	98.73114		6,6	0.26638	5,5	0.22223	0,0	0.17347	0.19969	1.81821	
59	99.68387		5,5	0.33968	0,0	0.20227	6,6	0.19941	0.27965	1.68349	
60	100.63525	0.98045	5	5,5	0.49277	0,0	0.21973	6,6	0.13320	0.44666	1.42236
61	101.62990		6,6	0.45397	1,1	0.22843	5,5	0.09139	0.40433	1.55209	
62	102.64995		6,6	0.41259	0,0	0.14677	5,5	0.10603	0.35918	1.69092	

63	103.66118	6,6	0.41207	5,5	0.14829	0,0	0.13460	0.35862	1.69677
64	104.61332	1,1	0.34839	7,7	0.28352	4,4	0.12550	0.28915	1.63494

TABLE VII: Many-body ground state energies in Lab frame, E_0^{lab} , for $N=16$ bosons interacting via finite range Gaussian potential given in Eq. (1), with interaction strength $g_2 = 0.9151$ and interaction range $\sigma = 0.50$. The three largest macroscopic eigenvalues $\lambda_1 > \lambda_2 > \lambda_3$ of the SPRDM, corresponding single particle quantum numbers (n_1, m_1) , (n_2, m_2) and (n_3, m_3) respectively, degree of condensation C_d and von-Neumann entropy S_1 are calculated from SPRDM in Eq. (14) along with critical angular velocity Ω_c and p -fold symmetry in the total angular momentum space ranging from $0 \leq L_z \leq 4N$ are noted below in beyond LLL $n_r = 1$.

L_z	$E_0^{Lab}(L_z)$	Ω_c	p	(n_1, m_1)	λ_1	(n_2, m_2)	λ_2	(n_3, m_3)	λ_3	C_d	S_1
0	46.35902	0	-	0,0	0.99292	1,-1	0.00278	1,1	0.00278	0.99213	0.05181
1	47.36087			0,0	0.92678	1,1	0.06622	1,-1	0.00485	0.91865	0.29272
2	48.08484			0,0	0.92363	2,2	0.05542	1,1	0.01677	0.91515	0.33062
3	48.81060			0,0	0.91811	3,3	0.05051	1,1	0.01665	0.90902	0.37195
4	49.73297			0,0	0.83691	1,1	0.08557	2,2	0.05098	0.81879	0.62421
5	50.48376			0,0	0.82582	2,2	0.06967	1,1	0.06365	0.80646	0.66569
6	51.25036			0,0	0.81479	3,3	0.07857	1,1	0.06500	0.79422	0.69206
7	52.08038			0,0	0.71652	1,1	0.15698	2,2	0.08601	0.68503	0.88604
8	52.84751			0,0	0.67944	1,1	0.17796	2,2	0.09439	0.64382	0.95372
9	53.62127			0,0	0.62186	1,1	0.23161	2,2	0.09790	0.57984	1.02310

10	54.39106		0,0	0.54967	1,1	0.30222	2,2	0.11176	0.49964	1.06854	
11	55.15183		0,0	0.48501	1,1	0.36641	2,2	0.11592	0.42779	1.09168	
12	55.90975		1,1	0.44355	0,0	0.41282	2,2	0.11674	0.38172	1.08372	
13	56.66452		1,1	0.53037	0,0	0.33575	2,2	0.11280	0.47818	1.03877	
14	57.41706		1,1	0.63071	0,0	0.25192	2,2	0.10200	0.58967	0.94210	
15	58.16768		1,1	0.74901	0,0	0.15910	2,2	0.08204	0.72113	0.76514	
16	58.90377	0.78405	-	1,1	0.87949	0,0	0.06083	2,2	0.05387	0.86853	0.47622
17	59.90512		1,1	0.72520	2,2	0.14895	0,0	0.11138	0.70022	0.83373	
18	60.87598		1,1	0.65539	2,2	0.16395	0,0	0.13487	0.62406	1.02094	
19	61.70337		1,1	0.74832	2,2	0.09687	0,0	0.08710	0.72544	0.88665	
20	62.66299		1,1	0.56506	2,2	0.21911	0,0	0.14556	0.52552	1.17825	
21	63.59491		1,1	0.40591	2,2	0.31222	0,0	0.20091	0.35190	1.32012	
22	64.46708		1,1	0.41047	2,2	0.29314	0,0	0.19153	0.35688	1.35405	
23	65.38521		2,2	0.38009	1,1	0.30566	0,0	0.20860	0.32373	1.37516	
24	66.25488		2,2	0.52244	0,0	0.27979	1,1	0.27979	0.47903	1.21842	
25	67.19100		2,2	0.43787	1,1	0.21557	0,0	0.20891	0.38676	1.39541	
26	68.04368		2,2	0.57653	0,0	0.24110	4,4	0.07248	0.53803	1.17032	
27	69.02539		2,2	0.49911	0,0	0.18611	1,1	0.15505	0.45357	1.35454	
28	69.86716	0.91362	2	2,2	0.61129	0,0	0.19537	4,4	0.07853	0.57595	1.15285
29	70.88586		2,2	0.47026	0,0	0.18210	3,3	0.17080	0.42211	1.39336	
30	71.73464		2,2	0.63313	0,0	0.15321	3,3	0.09048	0.59978	1.14251	
31	72.76240		2,2	0.44022	3,3	0.20842	0,0	0.17746	0.38933	1.42515	
32	73.59262	0.93136	2	2,2	0.48124	0,0	0.16906	4,4	0.13125	0.43408	1.47162
33	74.54991		2,2	0.30196	0,0	0.21557	3,3	0.19393	0.23851	1.68952	
34	75.48376		3,3	0.25519	2,2	0.25365	0,0	0.22252	0.18748	1.66507	

35	76.41198		3,3	0.31683	0,0	0.23683	2,2	0.19349	0.25472	1.63755	
36	77.34967	0.93926	3	3,3	0.48347	0,0	0.23920	2,2	0.18098	0.43652	1.41417
37	78.32315		3,3	0.27538	0,0	0.21411	2,2	0.20491	0.20950	1.71124	
38	79.26053		3,3	0.36638	0,0	0.21275	2,2	0.16164	0.30878	1.61267	
39	80.19670		3,3	0.47883	0,0	0.20164	4,4	0.12226	0.43146	1.45707	
40	81.18208		0,0	0.23981	4,4	0.22654	3,3	0.18993	0.17070	1.73263	
41	82.14866		3,3	0.32007	0,0	0.19086	4,4	0.16184	0.25826	1.67613	
42	83.09047		3,3	0.38254	0,0	0.18530	4,4	0.16036	0.32641	1.61470	
43	84.05134		4,4	0.33797	0,0	0.24222	3,3	0.17261	0.27778	1.61750	
44	84.99470		4,4	0.43838	0,0	0.25920	5,5	0.10867	0.38733	1.46766	
45	86.00803		4,4	0.25919	0,0	0.24227	5,5	0.23546	0.19184	1.66284	
46	86.97846		4,4	0.27755	5,5	0.19614	0,0	0.19235	0.21188	1.69785	
47	87.91174		4,4	0.37577	0,0	0.20809	5,5	0.16238	0.31902	1.57633	
48	88.73774	0.94901	4	4,4	0.47930	0,0	0.21845	3,3	0.11075	0.43196	1.49457
49	89.76270		4,4	0.32100	0,0	0.21662	5,5	0.17762	0.25927	1.69756	
50	90.74682		4,4	0.23463	3,3	0.20335	0,0	0.19545	0.16505	1.82869	
51	91.70336		4,4	0.29217	3,3	0.21128	0,0	0.17811	0.22782	1.75395	
52	92.64065	0.97573	4	4,4	0.54190	0,0	0.17028	3,3	0.09559	0.50026	1.41701
53	93.65995		4,4	0.30013	5,5	0.19670	0,0	0.17472	0.23651	1.74607	
54	94.64215		5,5	0.22788	0,0	0.21393	3,3	0.21335	0.15769	1.78591	
55	95.61163		5,5	0.41169	0,0	0.2505	6,6	0.12700	0.35821	1.57743	
56	96.59324		6,6	0.32819	1,1	0.19334	0,0	0.12312	0.26711	1.79390	
57	97.59379		6,6	0.27007	5,5	0.22202	0,0	0.17065	0.20371	1.82421	
58	98.57570		6,6	0.25901	5,5	0.22335	0,0	0.17368	0.19165	1.81728	
59	99.53192		5,5	0.34524	0,0	0.20254	6,6	0.19324	0.28572	1.67410	

60	100.48698	0.98079	5	5,5	0.50136	0,0	0.22034	6,6	0.12698	0.45602	1.40314
61	101.48789			6,6	0.42762	1,1	0.20063	5,5	0.12101	0.37558	1.61835
62	102.50076			6,6	0.40369	5,5	0.15460	0,0	0.14726	0.34948	1.69947
63	103.50724			6,6	0.39121	5,5	0.16719	0,0	0.12877	0.33587	1.71905
64	104.46445			1,1	0.31898	7,7	0.24512	4,4	0.14863	0.25707	1.71422

TABLE VIII: Many-body ground state energies in Lab frame, E_0^{lab} , for $N=16$ bosons interacting via finite range Gaussian potential given in Eq. (1), with interaction strength $g_2 = 0.9151$ and interaction range $\sigma = 0.75$. The three largest macroscopic eigenvalues $\lambda_1 > \lambda_2 > \lambda_3$ of the SPRDM, corresponding single particle quantum numbers (n_1, m_1) , (n_2, m_2) and (n_3, m_3) respectively, degree of condensation C_d and von-Nuemann entropy S_1 are calculated from SPRDM in Eq. (14) along with critical angular velocity Ω_c and p -fold symmetry in the total angular momentum space ranging from $0 \leq L_z \leq 4N$ are noted below in beyond LLL $n_r = 1$.

L_z	$E_0^{Lab}(L_z)$	Ω_c	p	(n_1, m_1)	λ_1	(n_2, m_2)	λ_2	(n_3, m_3)	λ_3	C_d	S_1
0	45.36785	0.0	-	0,0	0.99664	1,1	0.00146	1,-1	0.00146	0.99627	0.02637
1	46.36791			0,0	0.93204	1,1	0.06462	1,-1	0.00263	0.92448	0.26448
2	47.08297			0,0	0.92901	2,2	0.05695	1,1	0.01227	0.92112	0.29870
3	47.87304			0,0	0.92162	3,3	0.05066	1,1	0.01533	0.91291	0.35101
4	48.77732			0,0	0.84923	2,2	0.08871	1,1	0.05363	0.83248	0.55652
5	49.56409			0,0	0.83417	2,2	0.07245	1,1	0.05350	0.81574	0.63424
6	50.38120			0,0	0.81743	3,3	0.07690	1,1	0.06302	0.79714	0.67842

7	51.22436		0,0	0.72779	2,2	0.13523	2,2	0.10344	0.69755	0.85740	
8	52.03192		0,0	0.68952	1,1	0.16253	2,2	0.10159	0.65502	0.93344	
9	52.84731		0,0	0.62580	1,1	0.22300	2,2	0.10954	0.58423	1.00928	
10	53.65663		0,0	0.55727	1,1	0.28850	2,2	0.12212	0.50808	1.05753	
11	54.46197		0,0	0.48999	1,1	0.35737	2,2	0.12412	0.43333	1.08301	
12	55.26553		1,1	0.43835	0,0	0.41559	2,2	0.12329	0.37594	1.07531	
13	56.06727		1,1	0.52917	0,0	0.33649	2,2	0.11684	0.47686	1.02898	
14	56.86801		1,1	0.63353	0,0	0.25064	2,2	0.10350	0.59281	0.92839	
15	57.66821		1,1	0.75436	0,0	0.15669	2,2	0.08146	0.72707	0.74679	
16	58.46294	0.81844	-	1,1	0.88316	0,0	0.05944	2,2	0.05	0.87254	0.45850
17	59.46389		1,1	0.72910	2,2	0.14918	0,0	0.10962	0.70447	0.81661	
18	60.41157		1,1	0.68344	2,2	0.13243	0,0	0.12793	0.65466	0.98546	
19	61.26707		1,1	0.76392	2,2	0.09034	0,0	0.08000	0.74246	0.84582	
20	62.23797		1,1	0.58188	2,2	0.21401	0,0	0.13675	0.54387	1.14812	
21	63.16968		1,1	0.45490	2,2	0.27007	0,0	0.18285	0.40535	1.31036	
22	64.05903		1,1	0.51903	2,2	0.22401	0,0	0.14461	0.47531	1.27725	
23	64.99627		2,2	0.36228	1,1	0.34470	0,0	0.18875	0.30431	1.36103	
24	65.89361		2,2	0.51307	0,0	0.26090	1,1	0.13135	0.46881	1.24812	
25	66.82809		2,2	0.40627	1,1	0.26644	0,0	0.18659	0.35229	1.40786	
26	67.71570		2,2	0.58305	0,0	0.22595	1,1	0.08725	0.54514	1.17153	
27	68.68383		2,2	0.49899	1,1	0.18282	0,0	0.16587	0.45345	1.34291	
28	69.55952	0.92471	2	2,2	0.62821	0,0	0.17685	1,1	0.07645	0.594421	1.13237
29	70.55437		2,2	0.50003	1,1	0.15967	3,3	0.14859	0.45458	1.35407	
30	71.43247	0.93648	2	2,2	0.67711	0,0	0.12229	1,1	0.07103	0.64776	1.06564
31	72.44891		2,2	0.48912	3,3	0.20769	0,0	0.14204	0.44268	1.35549	

32	73.31758	0.94256	2	2,2	0.63923	3,3	0.09346	1,1	0.09329	0.60644	1.18693
33	74.29530			2,2	0.35610	3,3	0.24362	0,0	0.19006	0.29757	1.57845
34	75.24622			2,2	0.29534	3,3	0.24975	0,0	0.19127	0.23128	1.63970
35	76.18597			3,3	0.25519	2,2	0.25365	0,0	0.22252	0.18748	1.62212
36	77.12801	0.95261	3	3,3	0.50812	0,0	0.23021	2,2	0.10629	0.46340	1.36944
37	78.10569			3,3	0.31124	2,2	0.20665	0,0	0.19600	0.24863	1.68195
38	79.05078			3,3	0.38258	0,0	0.19200	2,2	0.17805	0.32646	1.58994
39	79.98856	0.95352	3	3,3	0.53684	0,0	0.18769	4,4	0.09989	0.49474	1.35894
40	80.98327			3,3	0.35689	0,0	0.18428	2,2	0.14831	0.29843	1.65862
41	81.94333			3,3	0.36876	0,0	0.17156	2,2	0.16218	0.31138	1.62475
42	82.88402			3,3	0.53418	0,0	0.14530	4,4	0.11736	0.49183	1.40346
43	83.86494			4,4	0.29744	3,3	0.23747	0,0	0.20865	0.23357	1.65447
44	84.82073			4,4	0.39876	0,0	0.23720	3,3	0.14083	0.34411	1.55038
45	85.81515			3,3	0.49713	4,4	0.16417	0,0	0.10927	0.45141	1.47099
46	86.78861			4,4	0.25276	3,3	0.21999	5,5	0.18615	0.18483	1.71751
47	87.73690			4,4	0.36723	0,0	0.19508	3,3	0.17510	0.30970	1.59510
48	88.60174	0.95702	4	4,4	0.46760	0,0	0.21079	3,3	0.11811	0.41920	1.52696
49	89.62116			4,4	0.32397	0,0	0.21245	5,5	0.17784	0.26252	1.69957
50	90.59611			4,4	0.37857	3,3	0.15893	0,0	0.15433	0.32207	1.73414
51	91.55611			4,4	0.32979	3,3	0.21110	0,0	0.16150	0.26886	1.71583
52	92.50030	0.97464	4	4,4	0.53680	0,0	0.16591	3,3	0.09784	0.49469	1.43474
53	93.51604			4,4	0.32485	5,5	0.19984	0,0	0.16602	0.26347	1.71963
54	94.50029			4,4	0.29504	0,0	0.19093	5,5	0.18550	0.23095	1.76970
55	95.47868			5,5	0.39847	0,0	0.23822	4,4	0.11948	0.34378	1.60971
56	96.44362			4,4	0.53301	0,0	0.11707	5,5	0.11096	0.49056	1.48399

57	97.45045		5,5	0.34580	0,0	0.17726	6,6	0.14997	0.28632	1.75599	
58	98.43219		6,6	0.22502	4,4	0.21346	5,5	0.20474	0.15457	1.82065	
59	99.39629		5,5	0.34703	0,0	0.19718	6,6	0.18262	0.28767	1.67528	
60	100.35792	0.98220	5	5,5	0.50544	0,0	0.21727	6,6	0.12034	0.46049	1.39901
61	101.36445		6,6	0.36603	5,5	0.18254	1,1	0.14930	0.30840	1.71183	
62	102.36492		6,6	0.28829	5,5	0.28503	0,0	0.13531	0.22358	1.74530	
63	103.36137		6,6	0.32674	5,5	0.22540	0,0	0.11743	0.26553	1.76037	
64	104.31541		1,1	0.25069	4,4	0.19113	5,5	0.17554	0.18257	1.81939	

-
- [1] Alex Andriati, Leonardo Brito, Lauro Tomio, and Arnaldo Gammal Phys. Rev. A **104**, 033318 (2021).
- [2] M. H. Anderson, J. R. Ensher, M. R. Matthews, C. E. Wieman, E. A. Cornell, Science **198**, 269, (1995).
- [3] M. R. Andrews, M-O. Mewes, N.J. van Druten, D. S. Durfee, D. M. Kurn, and W. Ketterle, Science **273**, 84 (1996).
- [4] F. Dalfovo, S. Giorgini, L. P. Pitevskii, and S. Stringari, Rev. Mod. Phys. **71**, 463 (1999).
- [5] L. Salasnich, A. Parola and L. Reatto, Phys. Rev. A **59**, 2990 (1999).
- [6] L. Salasnich, A. Parola and L. Reatto, Phys. Rev. A **60**, 04171 (1999).
- [7] Jakub Kopycinski, Wojcie R. Pudelko and Gabriel Wlazlowski [arXiv:2109.00427v1], (2019).
- [8] Alex Andriati, Leonardo Brito, Lauro Tomio, and Arnaldo Gammal, Phys. Rev. A **104**, 033318 (2021)
- [9] Roger R. Sakhel, Asaad R. Sakhel, J Low Temp Phys **184** 1092–1113 (2016).

- [10] N. R. Cooper and N. K. Wilkin Phys. Rev. B **60**, 16279 (1999).
- [11] G. Eriksson, J. Bengtsson, G. M. Kavoulakis, and S. M. Reimann, Phys. Rev. A, **100**, 063638 (2019).
- [12] R. J. Donnelly, Quantized Vortices in Helium II (Cambridge University Press, Cambridge, 1991).
- [13] D. S. Rokhsar, Phys. Rev. Lett, **79**, 2164 (1997).
- [14] Xia-Ji Liu, Hui Hu, Lee Chang, Weiping Zhang, Shi-Qun Li, and Yu-Zhu Wang, Phys. Rev A, **87**, 030404 (2001).
- [15] C.C Bradley, C.A Sackett, J.J. Toilett, and R.G. Hulet, Phys. Rev. Lett. **75**, 1687 (1995).
- [16] M. R. Matthews, B. P. Anderson, P. C. Haljan, D. S. Hall, C. E. Wieman, and E. A. Cornell, Phys. Rev. Lett. **83**, 2498 (1999).
- [17] D. Durkin and J. Fajans, Phys. Rev. Lett. **85**, 4052 (2000).
- [18] Ana Maria Rey. Rev. Acad. Colomb.(2021).
- [19] K.W. Madison, F. Chevy, W. Wohlleben, and J. Dalibard, Phys. Rev. Lett. **84**, 806 (2000).
- [20] Q. Guan, V. Klinkhamer, R. Klemt, J. H. Becher, A. Bergschneider, P. M. Preiss, S. Jochim, and D. Blume, Phys. Rev. Lett. **122**, 083401 (2019).
- [21] S. Inouye, M.R. Andrews, J.Stanger, H.J.Miesner, D.M. Stamper-Kurn and W. Ketterle, Nature (London) **392**,(1998) 151.
- [22] A.D.Lange, K.Pilch, A. Pranter, F.Ferlaino, B. Engeser, H.-C. Nägerl, R. Grsimm and C. Chin,Phys. Rev A, **79**, 013622 (2009).
- [23] Luca Salasnich and Boris A. Malomed, Phys. Rev. A **79**, 053620 (2009).
- [24] Xia-Ji Liu, Hui Hu, Lee Chang and Shi-Qun Li, Phys. Rev A, **64**, 035601 (2001).
- [25] Dingping Li, Phys. Rev B, **60**, 9704 (2019).
- [26] Gentaro Watanabe, Gordon Baym and C. J. Pethick , Phys. Lett. **122**, 235301 (2019).

- [27] Sergej Moroz and Dam Thanh Son, Phys. Lett. **93**, 190401 (2004).
- [28] Rostislav A. Doganov, Shachar Klaiman, Ofir E. Alon, Alexej I. Streltsov and Lorenz S. Cederbaum, Phys. Rev A **87**,033631-1 (2013).
- [29] Peter Jeszenszki. Ali. Alavi and Joachin Brand, Phys. Rev. A **99**, 033608 (2019).
- [30] M. A. H. Ahsan and N. Kumar, Phys. Rev. A **64**, 013608 (2001).
- [31] A. A. Abrikosov, Revs. of Mod Phys. **76**, 0975 (2004).
- [32] Chuan-Yin Xia, Hua-Bi Zeng, Yu Tian, Chiang-Mei Chen and Jan Zaanen, Phys. Rev D, **105**, L021901 (2022).
- [33] F. Dalfovo and S. Stringari, Phys. Rev A **53**, 2477 (2018).
- [34] Przemyslaw Koscik and Tomasz. Sowinsk. Scientific reports **8**,18505 (2018).
- [35] Thomas Thomas, Berthold-Georg Englert, Kazimierz Rzazewski and Kazimierz Wilkens. Foundations of Physics,**549**, 498 (1997).
- [36] Pere Mujal, Artur Polls and B Juliä-Díaz, Phys. Rev. Lett., **97**, 063618, (2018).
- [37] Shachar Klaiman, Nimrod Moiseyev and Lorenz S Cederbaum. Phys. Rev. A **73**, 013622 (2006).
- [38] C. J. Pethick and H. Smith (Cambridge University Press, Cambridge, 2002).
- [39] G. Baym and C. J. Pethick, Phys. Rev. Lett., **76**, 6 (1996).
- [40] N.K. Wilkin, and JMF Gunn, Phys. Rev. Lett. **84**, 6 (2000).
- [41] N. Barberán, M. Lewenstein, K. Osterloh, and D. Dagnino, Phys. Rev A, **73**, 063623 (2006).
- [42] Zho Liu, Hongli Guo, Shu Chen, and Heng Fan, Phys. Rev A, **80**, 063606 (2009).
- [43] Richard E. Prange, Steven M. Girvin ,The quantum Hall effect, (2e) (Springer-Verlag, 1990).
- [44] Alexander L. Fetter Phys. Rev. A, **64**, 063608 (2001).
- [45] Leonardo Brito, Alex Andriati, Lauro Tomio, and Arnaldo Gammal, Phys. Rev A **102**, 063330 (2020).

- [46] O. Penrose, *Philos. Mag.* **42**, 1373 (1951).
- [47] L. D. Landau and E. M. Lifshitz, *Statisticheskaya Fizika (Fiz- matgiz, Moscow, 1951); Statistical Physics Pergamon, Ox- ford, 1958, Chap. 133.*
- [48] O. Penrose and L. Onsager, *Phys. Rev.* **104**, 576 (1956).
- [49] C. J. Pethick and L. P. Pitaevskii, *Phys. Rev. A*, **53**, 2477 (2018).
- [50] C. N. Yang, *Rev. Mod. Phys.* **34**, 4 (1962).
- [51] Erich J. Mueller Tin-Lun Ho, Masahito Ueda, and Gordon Baym *Phys. Rev. A*, **74**, 033612 (2006).
- [52] Daniele Dimonte and Marco Falconi and Alessandro Olgiati, *IOP*, **34**, 1-32 (2020).
- [53] Gabriel T. Landi, and Mauro Paternostro, *Revs. of Mod. Phys.* **62**, 033609 (2000).
- [54] R. Paškauskas and L. You, *Phys. Rev. A* **64**, 042310 (2001).
- [55] J. Eisert, M. Cramer, and M. B. Plenio, *Rev. Mod. Phys.* **82**, 277 (2010).
- [56] Nicolas Laflorencie, *Physics Reports*, **646**, 1-59 (2016).
- [57] N. Sánchez-Kuntz, and S. Floerchinger, *Phys. Rev. A* **103**, 063606 (2021).
- [58] B Juliä-Díaz, D. Dagnino, K. J. Günter, T. Graß, N. Barber 'an, M. Lewenstein, and J. Dalibard, *Phys. Rev. A*, **84**, 053605 (2011).
- [59] K. K Witkowski and T. K. Kope 'c *J. Low Temp. Phys.* **201** 340 (2020)
- [60] Chien-Nan Liu, Akiyoshi Hishikawa, and Toru Morishita, *Phys. Rev. A* **86**, 053426 (2012).
- [61] F. Cajiao Vélez, Lei Geng, J. Z. Kamiński, Liang-You Peng, and K. Krajewska, *Phys. Rev. A* **102**, 043102 (2020).
- [62] Constantine Yannouleas and Uzi Landman, *Phys. Rev. A* **85**, 1726 (2000).
- [63] Jerzy Cioslowski, *J. Phys. B: At. Mol. Opt. Phys.* **50** (2017) 235102
- [64] H. Saarikoski, S. Reimann, A. Harju, and M. Manninen, *Rev. Mod. Phys.* **82**, 2785 (2010).
- [65] Tatsuya Nakajima, and Masahito Ueda, *Phys. Rev. Lett.* **91**, 140401 (2003).

- [66] G. M. Kavoulakis, S. M. Reimann, and B. Mottelson, *Phys. Rev. Lett.*, **89**, 079403 (2002).